

COMPUTATIONAL GRAPH COMPLETION

HOUMAN OWHADI

ABSTRACT. We introduce a framework for generating, organizing, and reasoning with computational knowledge. It is motivated by the observation that most problems in Computational Sciences and Engineering (CSE) can be described as that of completing (from data) a computational graph representing dependencies between functions and variables. Functions and variables may be known, unknown, or random. Data comes in the form of observations of distinct values of a finite number of subsets of the variables of the graph (satisfying its functional dependencies). The underlying problem combines a regression problem (approximating unknown functions) with a matrix completion problem (recovering unobserved variables in the data). Replacing unknown functions by Gaussian Processes (GPs) and conditioning on observed data provides a simple but efficient approach to completing such graphs. Since the proposed framework is highly expressive, it has a vast potential application scope. Since the completion process can be automatized, as one solves $\sqrt{\sqrt{2} + \sqrt{3}}$ on a pocket calculator without thinking about it, one could, with the proposed framework, solve a complex CSE problem by drawing a diagram. Compared to traditional regression/kriging, the proposed framework can be used to recover unknown functions with much scarcer data by exploiting interdependencies between multiple functions and variables. The Computational Graph Completion (CGC) problem addressed by the proposed framework could therefore also be interpreted as a generalization of that of solving linear systems of equations to that of approximating unknown variables and functions with noisy, incomplete, and nonlinear dependencies. Numerous examples illustrate the flexibility, scope, efficacy, and robustness of the CGC framework and show how it can be used as a pathway to identifying simple solutions to classical CSE problems. These examples include the seamless CGC representation of known methods (for solving/learning PDEs, surrogate/multiscale modeling, mode decomposition, deep learning) and the discovery of new ones (digital twin modeling, dimension reduction).

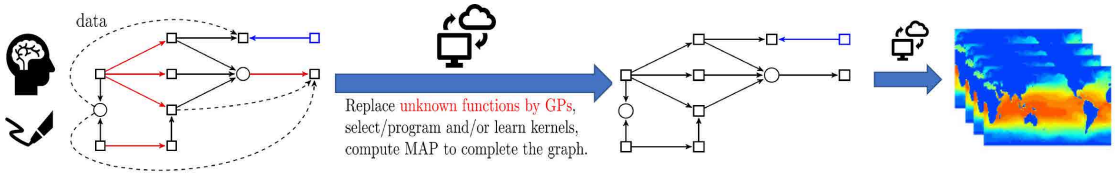
1. Introduction

1.1. Motivations. The complexity of a problem is relative to our ability to decompose it by reasoning through simple concepts encapsulating and abstracting away its intricacies and technicalities. For example, (1) computing $\sqrt{\sqrt{2} + \sqrt{3}}$ is a complex task if one tries to solve it by hand and a simple one if one uses a pocket calculator, (2) calculating a mortgage amortization schedule is a complex task if done by hand and a simple one if done with an Excel sheet, (3) designing an engine valve is a complex task if done by hand and a simple one if done with AutoCAD. Why? Because the technicalities and intricacies have been abstracted away, and the user is only left with the task of manipulating simple/high-level concepts. Many problems in Computational Sciences

Date: June 4, 2022.

Caltech, MC 9-94, Pasadena, CA 91125, USA, owhadi@caltech.edu.

and Engineering (CSE) are seen as complex because they involve intricate interplays between multiple physics, multiple scales, nonlinear effects, missing/partial information, and limited resources (in human time and expertise). Can the complexities of most of these problems be abstracted away? Can the underlying problems be reduced to that of manipulating simple, high-level concepts and relations? An affirmative answer to these questions would lead to a paradigm shift in which most CSE problems are solved through high-level operations without thinking about them. The purpose of this manuscript is to introduce a rigorous and unified framework reducing CSE problems to the completion of computational graphs representing dependencies between (known, unknown or random) functions and variables. Replacing unknown functions with Gaussian processes and conditioning on available data/measurements provide a simple but powerful tool for solving Computational Graph Completion (CGC) problems when the underlying kernels are also learned from data [29] or programmed [28] for the task at hand. Since this completion process can be automatized, as one solves $\sqrt{\sqrt{2} + \sqrt{3}}$ on a pocket calculator without thinking about it, one could, with the proposed framework, solve a complex CSE problem by drawing a diagram (as illustrated below). This would accelerate innovation and decision making by enabling the real-time development and testing of models, ideas and scenarios.



As category theory has served as a mathematical model for breaking up mathematical models into their fundamental pieces analyzed through their (functorial) relationships, the proposed framework can serve as a model for breaking up CSE problems into their fundamental pieces and assembling them up through CGC. In that framework, creating a surrogate model for predicting the drag coefficient of a wing or extrapolating a time series could be seen as instances of the same problem (sharing the same CGC graph but solved with different kernels, variables, and data). As calculators free us up to perform tasks of greater importance, the automation of the proposed framework has the potential to free us to perform CSE tasks of significantly higher importance and complexity.

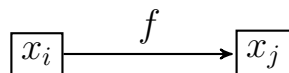
1.2. Outline of the article and properties of the framework. Sec. 2 describes the type of computational graphs used in this article. Sec. 2.5 introduces the notion of samples from the graph (variables of the graph satisfying its functional dependencies). Sec. 3 formulates the Computational Graph Completion (CGC) problem, which combines a regression problem (approximating unknown functions) with a matrix completion problem (recovering unobserved variables in the data). Sec. 4 illustrates the proposed problem and framework through the identification of the Digital Twin of a nonlinear electric circuit from scarce measurements. Sec. 5 presents the proposed Gaussian Process (GP) framework for solving the general CGC problem. This framework has several desirable properties: (1) it is highly expressive and has, therefore, a vast application scope, (2) it is interpretable and amenable to analysis, (3) its complexity reduces to that of kernel methods, (4) it is robust to data scarcity, (5) its regularization/stabilization is a rigorous

and a natural generalization of the regularization strategy employed in kriging, (6) it generalizes the notion of solving linear systems of equations to that of approximating unknown variables and functions with noisy, incomplete and nonlinear dependencies, (7) it can be automatized and can act as a pathway to identifying simple solutions to classical CSE problems. Sec. 6 illustrates the flexibility and scope of the proposed framework through examples related to solving nonlinear PDEs (Sec. 6.1), learning PDEs (Sec. 6.2), Deep Learning (Sec. 6.3, since training ANNs can naturally be formulated as a particular case of CGC, the proposed framework can naturally be employed to develop a theory for Deep Learning), the regularization of ANNs/ResNets (Sec. 6.4), dimension reduction (Sec. 6.5, including nonlinear active subspace learning in Sec. 6.5.3), mode decomposition (Sec. 6.6), empirical mode decomposition (Sec. 6.7), empirical mode decomposition with possibly unknown non-trigonometric waveforms (Sec. 6.8). Sec. 6.7 and Sec. 6.8 also show how the design of the graph can be made dynamic and include cycles.

2. Computational graphs

We will first describe the type of graphs used here and distinguish them from knowledge graphs, belief networks, and the type of computational graphs used for backpropagation. Knowledge graphs [9] (which have become critical to many enterprises today [21]) are composed of entities (e.g., universities, countries) as nodes and relationships (e.g. *is located in*) as directed edges. Their applications include data integration, its organization, and reasoning (through knowledge graph completion [18] which consists in completing the structure of knowledge graphs by predicting missing entities or relationships). Graphical models [17] (also known as belief/Bayesian networks) represent the conditional dependence structure between a set of random variables and enable reasoning and learning with complexity and uncertainty (through their encoded joint distribution). Traditional computation graphs [36] represent the flow of computation by organizing operations and variables into nodes linked by directed edges. They have recently become popular due to applications to backpropagation and automatic differentiation. For our purpose, we define a computational graph as a graph representing (functional) dependencies between a finite number of (not necessarily random) variables and functions. We will use nodes to represent variables and arrows to represent functions (in solid line) and data (in dashed line). We distinguish nodes used to aggregate variables by drawing them as circles. We will now introduce computational graphs through illustrative examples and then formally define such graphs.

2.1. Functional dependencies between variables. If a node representing a variable x_j has a single incoming solid arrow (representing a function f) from a node representing a variable x_i , then the corresponding diagram illustrated below



is interpreted as the following identity holding true

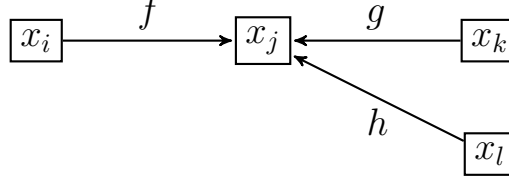
$$x_j = f(x_i). \quad (2.1)$$

2.2. Sums of variables. More generally, if a square node j representing a variable x_j has multiple incoming solid arrows from nodes i representing other variables x_i , then the

identity

$$x_j = \sum_{i \rightsquigarrow j} f_{i,j}(x_i), \quad (2.2)$$

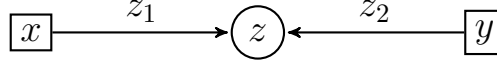
holds true for all values of the x_i , where we write $i \rightsquigarrow j$ for the set of nodes i with an outgoing solid arrow towards j and $f_{i,j}$ for the function represented by an arrow from i to j . Therefore, the following diagram



is interpreted as the identity

$$x_j = f(x_i) + g(x_k) + h(x_l). \quad (2.3)$$

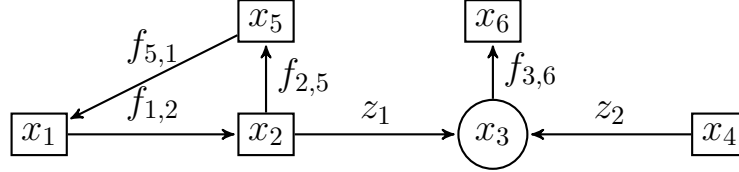
2.3. Aggregate variables. We will use circles for (and only for) variables obtained by aggregating other variables. For instance the following diagram



is interpreted as the identity

$$z = (x, y). \quad (2.4)$$

2.4. Functional dependencies. Therefore, we define a computational graph as a graph representing dependencies between a finite number of variables and functions. For instance the following diagram,



is interpreted as the following equations holding true: $x_2 = f_{1,2}(x_2)$, $x_3 = (x_2, x_4)$, $x_5 = f_{2,5}(x_2)$, $x_1 = f_{5,1}(x_5)$, $x_6 = f_{3,6}(x_3)$. Note that, contrary to traditional computational graphs, we allow for cycles, and the cycle in the above diagram can be interpreted as $f_{5,1} \circ f_{2,5} \circ f_{1,2}$ being the identity map.

2.5. General definition and samples from the graph. We generally (and formally) define a computational graph as (1) a collection of nodes/vertices \mathcal{V} , where each vertex in $i \in \mathcal{V}$ represents a variable x_i with values in a space \mathcal{X}_i , (2) combined with a collections of directed edges (arrows) $\mathcal{E} \subset \mathcal{V} \times \mathcal{V}$. \mathcal{V} is the disjoint union of \mathcal{V}_\square and \mathcal{V}_\circ where \mathcal{V}_\square is the set of square-shaped vertices, and \mathcal{V}_\circ is the set of circle-shaped vertices. For $e \in \mathcal{E}$, write $a(e)$ for the origin of the arrow e and $b(e)$ for its end point. If $b(e)$ is a square shaped vertex then e represents a function f_e mapping $\mathcal{X}_{a(e)}$ to $\mathcal{X}_{b(e)}$. Furthermore if j is a squared shaped vertex then the identity (2.2) holds true. If j is circle shaped vertex then the identity $x_j = \otimes_{i \rightsquigarrow j} x_i$ holds true, where $\otimes_{i \rightsquigarrow j} x_i$ represents the aggregation of variables with arrow from i to j (in that case, $\mathcal{X}_j = \otimes_{i \rightsquigarrow j} \mathcal{X}_i$). When necessary, the order of the aggregation is set by ordering the arrows ending in j as in Sec. 2.4. A collection of

variables $(X_i)_{i \in \mathcal{V}}$ satisfying the (functional and aggregation) constraints represented by the edges of the graph is called a *sample from the graph*.

3. The Computational Graph Completion problem

Let X_1, \dots, X_N be N samples from the graph where each $X_s = (X_{s,i})_{i \in \mathcal{V}}$ is a row vector whose entries are the values taken by the variables $(x_i)_{i \in \mathcal{V}}$ in sample s . Write $X := (X_{s,i})$ for the corresponding $= N \times \mathcal{V}$ matrix whose row s is X_s . Let M be a $N \times \mathcal{V}$ matrix with boolean entries in $\{0, 1\}$. Write

$$X[M] := \{X_{s,v} \mid M_{s,v} = 1\}, \quad (3.1)$$

for the subset of entries of X such that $M_{s,v} = 1$,

$$X[1 - M] := \{X_{s,v} \mid M_{s,v} = 0\}, \quad (3.2)$$

for the subset of entries of X such that $M_{s,v} = 0$.

We will now assume that some functions of the graph are unknown, write \mathcal{E}_u for the subset arrows representing unknown functions, and consider the following problem, which we will refer to as a Computational Graph Completion (CGC) problem.

Problem 1. *Given $X[M]$ (a partial observation of N samples from the graph) approximate the unknown functions $(f_e)_{e \in \mathcal{E}_u}$ and the unobserved variables $X[1 - M]$.*

Note that Problem 1 combines a regression problem (the approximation of the unknown functions $(f_e)_{e \in \mathcal{E}_u}$) with a matrix completion problem (the approximation of the missing entries of X in $X[M]$). Note also that for each sample s , only a (possibly nonconstant across samples) subset of the variables may be observed/measured.

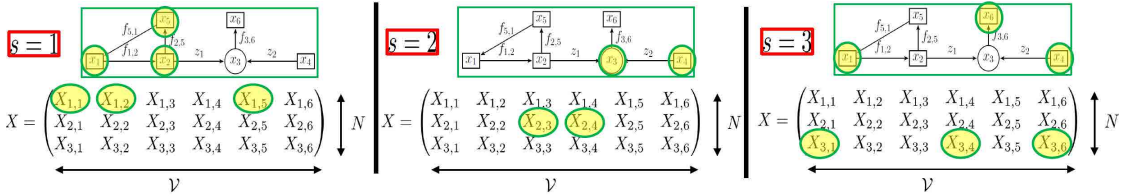
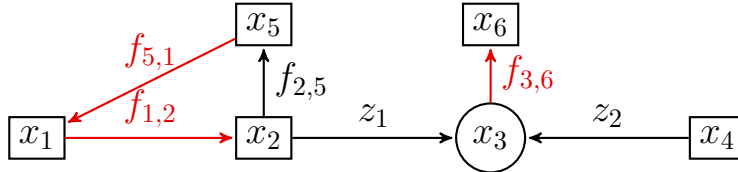


FIGURE 1. Observed variables in samples $s = 1, 2, 3$ from the graph.

As illustrated for the following diagram we will use red arrows to represent unknown functions and black arrows to represent known functions.



The following equation presents an instance of the matrices X and M for $N = 3$ and $|\mathcal{V}| = 6$ in the setting of the diagram above.

$$X = \begin{pmatrix} X_{1,1} & X_{1,2} & X_{1,3} & X_{1,4} & X_{1,5} & X_{1,6} \\ X_{2,1} & X_{2,2} & X_{2,3} & X_{2,4} & X_{2,5} & X_{2,6} \\ X_{3,1} & X_{3,2} & X_{3,3} & X_{3,4} & X_{3,5} & X_{3,6} \end{pmatrix} \quad M = \begin{pmatrix} 1 & 1 & 0 & 0 & 1 & 0 \\ 0 & 0 & 1 & 1 & 0 & 0 \\ 1 & 0 & 0 & 1 & 0 & 1 \end{pmatrix} \quad (3.3)$$

Fig. 1 shows the corresponding observed variables for samples $s = 1, 2, 3$.

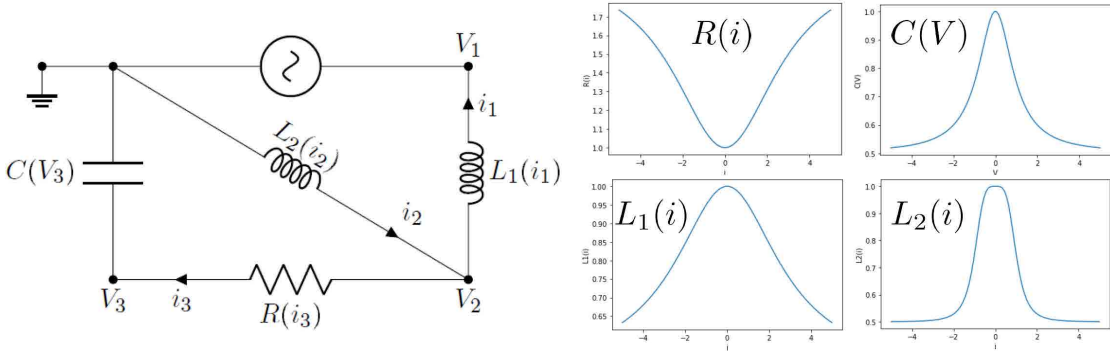


FIGURE 2. The nonlinear electric circuit.

4. Digital twin of an electric circuit from scarce measurements

We will now motivate Problem 1 by considering the problem of recovering the variables and physical laws of a nonlinear electric circuit from scarce noisy measurements (which could be seen as a simple example of Digital Twin modeling). Our solution for this particular example will also serve as a friendly introduction to the general solution to Problem 1 presented in Sec. 5.

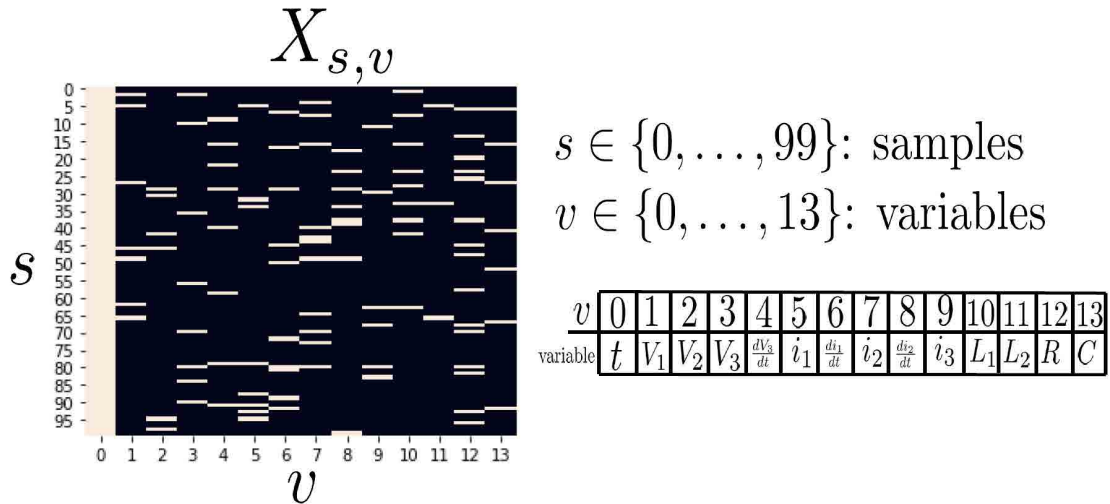


FIGURE 3. Observed entries of the matrix $X_{s,v}$ are colored in white.

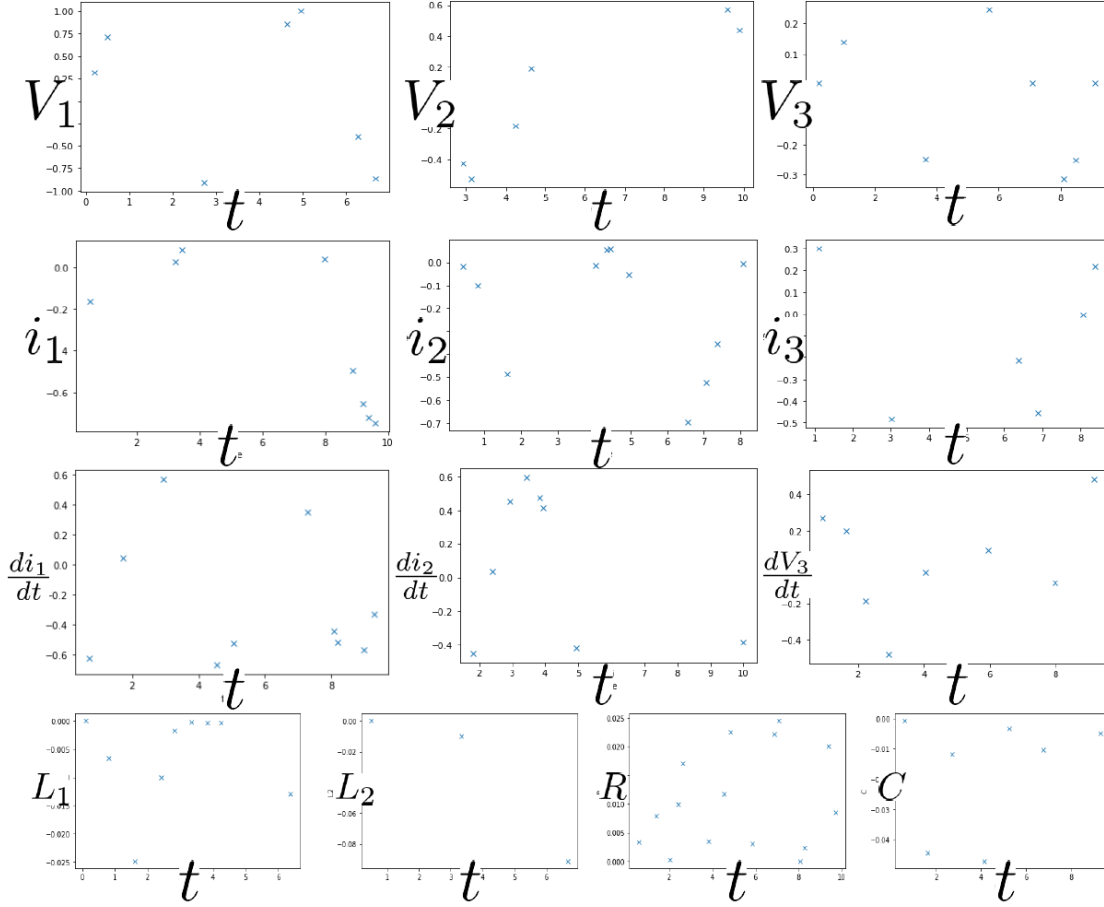


FIGURE 4. Values of $V_1, V_2, V_3, \frac{dV_3}{dt}, i_1, \frac{di_1}{dt}, i_2, \frac{di_2}{dt}, i_3, L_1, L_2, R, C$ at times when those variables are measured.

4.1. The problem. We consider the electric circuit drawn in Fig. 2. We assume that this circuit is nonlinear and that currents and voltages across the RLC components are related as shown in (4.2)-(4.5).

$$i_1 + i_3 = i_2 \quad (4.1)$$

$$i_3 = C(V_3) \frac{dV_3}{dt} \quad (4.2)$$

$$V_2 - V_3 = R(i_3) i_3 \quad (4.3)$$

$$-V_2 = L_2(i_2) \frac{di_2}{dt} \quad (4.4)$$

$$V_2 - V_1 = L_1(i_1) \frac{di_1}{dt}. \quad (4.5)$$

The functions $i \rightarrow R(i), L_1(i), L_2(i)$ and $V \rightarrow C(V)$ illustrated in Fig. 2 are assumed to be unknown. The time dependencies $t \rightarrow V_1(t), V_2(t), V_3(t), i_1(t), i_2(t), i_3(t)$ of all voltages and currents of the circuit are also assumed to be unknown. The circuit is run

for a given interval of time, and we seek to recover all unknown functions from scarce noisy measurements of its variables. To describe this we represent the state of the system by the value of the vector

$$x = (t, V_1, V_2, V_3, \frac{dV_3}{dt}, i_1, \frac{di_1}{dt}, i_2, \frac{di_2}{dt}, i_3, L_1, L_2, R, C) \quad (4.6)$$

where (see diagram in Fig. 2), $x_0 = t$ represents the current time, $x_1 = V_1$ represents the value $V_1(t)$ of the voltage V_1 at time $x_0 = t$, $x_5 = i_1$ represents the value $i_1(t)$ of the current i_1 at time $x_0 = t$, $x_6 = \frac{di_1}{dt}$ represents the value $\frac{di_1}{dt}(t)$ of the time derivative of the current i_1 at time $x_0 = t$, $x_{10} = L_1$ represents the value $L_1(i_1(t))$ of the inductance L_1 at time $x_0 = t$, $x_{13} = C$ represents the value $C(V_3(t))$ of the capacitance C at time $x_0 = t$. We run the circuit between $t = 0$ and $t = 10$ and, at times $t_s := \frac{s}{10}$ for $s \in \{0, 1, \dots, 99\}$, observe a random subset of the values of the variables representing the state of the system. To describe this, for $s \in \{0, \dots, 99\}$, let $(X_{s,v})_{0 \leq v \leq 13}$ be the value of the vector x at times t_s ($X_{s,0} = t_s$). Note that $(X_{s,v})_{0 \leq s \leq 99, 0 \leq v \leq 13}$ is a 100×14 matrix representing the values of all the variables of the system at times t_0, \dots, t_{99} . Let M be a 100×14 matrix with boolean entries in $\{0, 1\}$ such that $M_{s,v} = 1$ if the value of $X_{s,v}$ is measured/observed and $M_{s,v} = 0$ if the value of $X_{s,v}$ is not observed. For our experiments we select $M_{s,0} = 1$ for all s (we observe the value of the time variable at all times) and select the other entries to be independent identically distributed Bernoulli random variables such that (for $s \in \{0, \dots, 99\}$ and $v \in \{1, \dots, 13\}$) $M_{s,v} = 1$ with probability 0.07 (e.g. for each time t_s the probability that the value of V_1 is observed is 0.07).

Fig. 3 shows the observed entries of the matrix $X_{s,v}$. Fig. 4 shows the values of $V_1, V_2, V_3, \frac{dV_3}{dt}, i_1, \frac{di_1}{dt}, i_2, \frac{di_2}{dt}, i_3, L_1, L_2, R, C$ at times when those variables are measured. For instance (1) the V_1 plot in Fig. 4 shows the values of the function $t \rightarrow V_1(t)$ at times t_s such that $M_{s,1} = 1$, and (2) the C plot in Fig. 4 shows the values of the function $t \rightarrow C(i_3(t))$ at times t_s such that $M_{s,13} = 1$. Write

$$X[M] := \{X_{s,v} \mid M_{s,v} = 1\} \quad (4.7)$$

for the observed subset of the entries the matrix $X_{s,v}$ and consider the following problem.

Problem 2. *Given the partial measurements $X[M]$ approximate all the entries of the matrix $(X_{s,v})$ and all the functions $t \rightarrow V_1(t), V_2(t), V_3(t), \frac{dV_3}{dt}(t), i_1(t), \frac{di_1}{dt}(t), i_2(t), \frac{di_2}{dt}(t), i_3(t), i \rightarrow L_1(i), L_2(i), R(i)$ and $V \rightarrow C(V)$.*

Note that Problem 2 combines a matrix completion problem with a regression problem. Furthermore, the data available for approximating each individual function is much scarcer than in traditional regression problems. For instance, as shown in Fig. 4, the value of $t \rightarrow V_1(t)$ is only observed at seven points, and the proposed task is to recover V_1 everywhere. Fig. 4 should be compared with Fig. 7, which illustrates the true and predicted values of all variables with the method described below.

4.2. Graph representation of functional dependencies between variables. We will now use the (imperfectly known) functional dependencies between these variables to recover them at all times. In that sense, the proposed approach could be seen as a generalization of the problem of solving a system of linear equations to that of solving a system of imperfectly known and incomplete nonlinear equations. This is done in

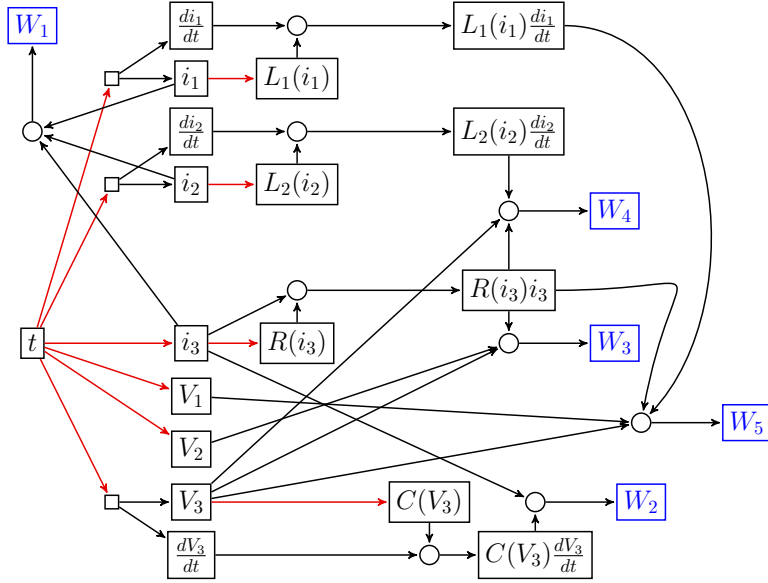
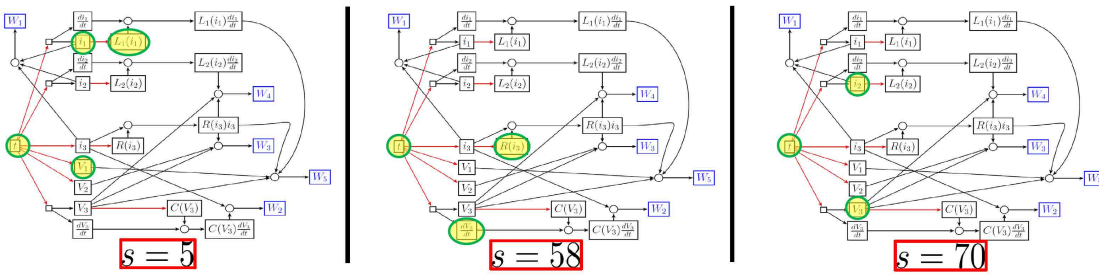


FIGURE 5. The computational graph.

the proposed CGC perspective by completing the computational graph drawn in Fig. 5 representing functional dependencies between variables with unknown functions (to be approximated) drawn in red. For the circuit drawn in Fig. 2 these functional dependencies correspond to the equations (4.1)-(4.5). The variables W_i illustrated in the above diagram are random variables described in Sec. 4.4 enabling a relaxation of the constraints imposed by equations (4.1)-(4.5). Note that for each known value of t , there are 13 unknown variables to be approximated and only 5 equations. Therefore the nonlinear system of equations under consideration is severely underdetermined. Fig. 6, highlights for samples $s = 5, 58, 70$, the nodes of the graph drawn in Fig. 5 that are associated with observed variables as indicated in Fig. 3.


 FIGURE 6. Observed variables in samples $s = 5, 58, 70$ from the graph.

4.3. Positivity of the unknown RLC parameters. To preserve the positivity of the unknown RLC parameters of the system, we consider the (also unknown) functions

$i \rightarrow l_1, l_2, r$, and $V \rightarrow c$ defined as the log the RLC functions, i.e.

$$C(V_3) = \exp(c(V_3)) \quad (4.8)$$

$$R(i_3) = \exp(r(i_3)) \quad (4.9)$$

$$L_2(i_2) = \exp(l_2(i_2)) \quad (4.10)$$

$$L_1(i_1) = \exp(l_1(i_1)). \quad (4.11)$$

We therefore introduce the modified matrix $(\bar{X}_{s,v})_{0 \leq s \leq 99, 0 \leq v \leq 13}$ defied by $\bar{X}_{s,v} := X_{s,v}$ for $v \notin \{10, \dots, 13\}$ and $\bar{X}_{s,v} := \log X_{s,v}$ for $v \in \{10, \dots, 13\}$.

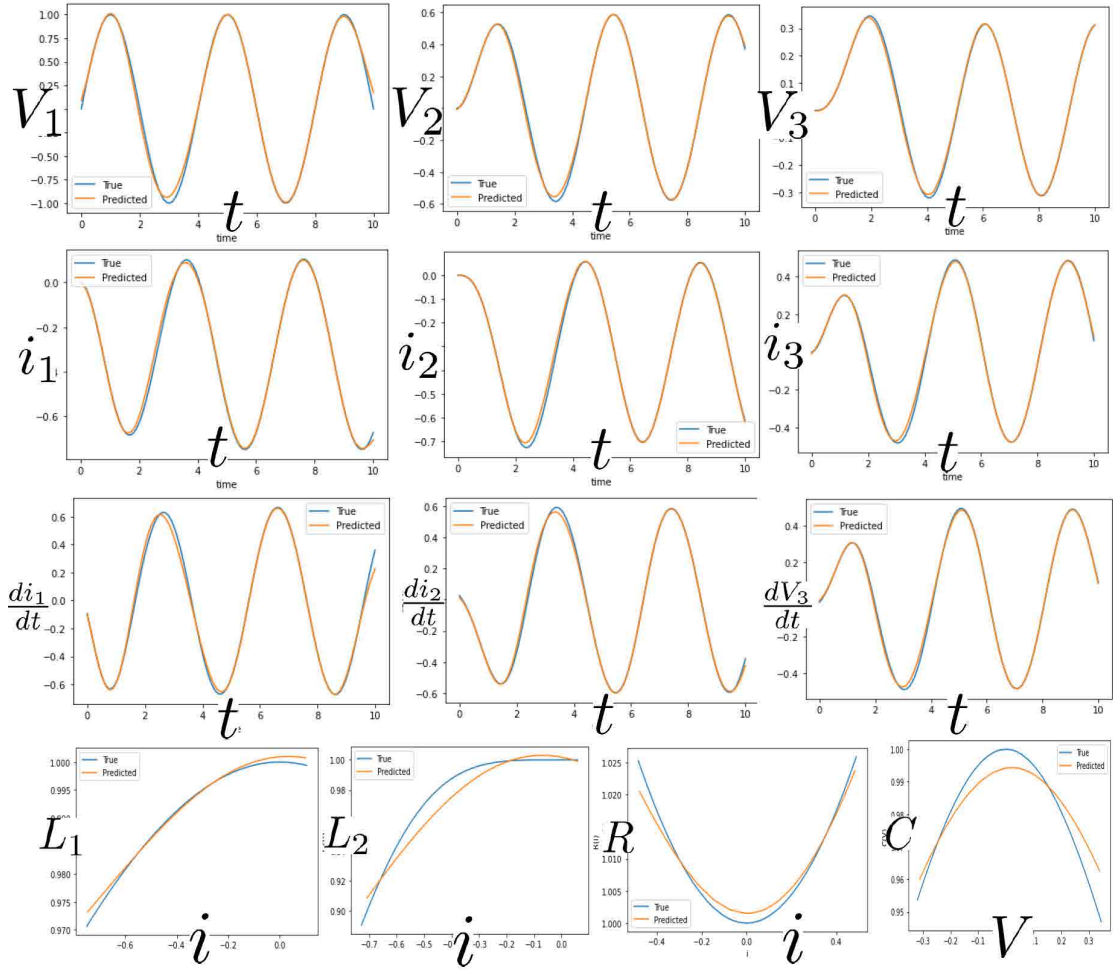


FIGURE 7. True values and recovered values of all variables.

4.4. The kernel based solution. Write $f := (V_1, V_2, V_3, i_1, i_2, i_3, l_1, l_2, r, c)$ for the unknown functions to be approximated and $Z := (Z_{s,v})_{0 \leq s \leq 99, 0 \leq v \leq 13}$ for our candidate for the approximation of \bar{X} . The proposed approach is then to compute f and Z by

minimizing the loss

$$\mathcal{L}(f, Z) := \|f\|^2 + \lambda_1 \mathcal{L}_1(f, Z) + \lambda_2 \mathcal{L}_2(Z) + \lambda_3 |Z[M] - \bar{X}[M]|^2, \quad (4.12)$$

over f and Z . In the expression (4.12), $\lambda_1, \lambda_2, \lambda_3$ are strictly positive parameters chosen to be 1000 in our numerical illustrations.

$$\|f\|^2 := \|V_1\|_K^2 + \|V_2\|_K^2 + \|V_3\|_K^2 + \|i_1\|_K^2 + \|i_2\|_K^2 + \|i_3\|_K^2 + \|l_1\|_K^2 + \|l_2\|_K^2 + \|r\|_K^2 + \|c\|_K^2$$

is the sum of RKHS norms of the functions $t \rightarrow V_1, V_2, V_3, i_1, i_2, i_3, i \rightarrow l_1, l_2, r$ and $V \rightarrow c$ with respect to the Gaussian kernel $K(a, a') := \exp(-|a - a'|^2)$. Write $|a|^2$ for the Euclidean norm of a when a is a vector and the Frobenius norm of a when a is matrix/tensor/array. $\mathcal{L}_1(f, Z)$ is a loss enforcing the dependencies between the unknowns functions f and variables Z . Those dependencies are allowed to be noisy and for the sake of clarity we did not represent all the noise variables in the computational graph drawn in Fig. 5.

$$\begin{aligned} \mathcal{L}_1(f, Z) := & |V_1(Z_{\cdot,0}) - Z_{\cdot,1}|^2 + |V_2(Z_{\cdot,0}) - Z_{\cdot,2}|^2 + |V_3(Z_{\cdot,0}) - Z_{\cdot,3}|^2 + \left| \frac{dV_3}{dt}(Z_{\cdot,0}) - Z_{\cdot,4} \right|^2 \\ & + |i_1(Z_{\cdot,0}) - Z_{\cdot,5}|^2 + \left| \frac{di_1}{dt}(Z_{\cdot,0}) - Z_{\cdot,6} \right|^2 + |i_2(Z_{\cdot,0}) - Z_{\cdot,7}|^2 + \left| \frac{di_2}{dt}(Z_{\cdot,0}) - Z_{\cdot,8} \right|^2 \\ & + |i_3(Z_{\cdot,0}) - Z_{\cdot,9}|^2 + |l_1(Z_{\cdot,5}) - Z_{\cdot,10}|^2 + |l_2(Z_{\cdot,7}) - Z_{\cdot,11}|^2 + |r(Z_{\cdot,9}) - Z_{\cdot,12}|^2 \\ & + |c(Z_{\cdot,13}) - Z_{\cdot,13}|^2 \end{aligned}$$

$\mathcal{L}_2(Z)$ is a loss enforcing the dependencies between the known functions and variables Z .

$$\begin{aligned} \mathcal{L}_2(Z) := & |Z_{\cdot,5} + Z_{\cdot,9} - Z_{\cdot,7}|^2 + |Z_{\cdot,9} - \exp(Z_{\cdot,13})Z_{\cdot,4}|^2 + |Z_{\cdot,2} - Z_{\cdot,3} - \exp(Z_{\cdot,12})Z_{\cdot,9}|^2 \\ & + |Z_{\cdot,2} + \exp(Z_{\cdot,11})Z_{\cdot,8}|^2 + |Z_{\cdot,2} - Z_{\cdot,1} - \exp(Z_{\cdot,10})Z_{\cdot,6}|^2. \end{aligned}$$

Note that the dependencies represented by \mathcal{L}_2 are also noisy and correspond to replacing (4.1)-(4.5) by the following equations in which the W_i (illustrated in the computational graph drawn in Fig. 5) are independent centered Gaussian random variables with variance $1/\lambda_2$.

$$i_1 + i_3 - i_2 = W_1 \quad (4.13)$$

$$i_3 - C(V_3) \frac{dV_3}{dt} = W_2 \quad (4.14)$$

$$V_2 - V_3 - R(i_3)i_3 = W_3 \quad (4.15)$$

$$-V_2 - L_2(i_2) \frac{di_2}{dt} = W_4 \quad (4.16)$$

$$V_2 - V_1 - L_1(i_1) \frac{di_1}{dt} = W_5. \quad (4.17)$$

Using the notations of (4.7), $|Z[M] - \bar{X}[M]|^2$ is the Euclidean norm of the difference between the $Z[M]$ and $\bar{X}[M]$. Note the last term in (4.12) enforces the constraints imposed by the observation of the data under the assumption that the data has been corrupted by i.i.d. noise (of centered Gaussian distribution with variance $1/\lambda_3$).

4.5. Reduction to a finite-dimensional optimization problem and numerical solution. For a given Z , (4.12) is quadratic in f and its minimizer (in f) can be computed explicitly as described in Sec. 5.7 (as a function of Z), e.g. (using vectorized notations) writing $\phi^1 = (\delta_{Z.,0})$, $\phi^2 = (\delta_{Z.,0} \circ \frac{d}{dt})$, $\phi = (\phi^1, \phi^2)$, the minimizer in i_1 is $i_1 = K(\cdot, \phi)(K(\phi, \phi) + \lambda_1^{-1}I)^{-1}(Z_{.,5}, Z_{.,6})$ and the value of $\|i_1\|_K^2 + \lambda_1(|i_1(Z_{.,0}) - Z_{.,5}|^2 + |\frac{di_1}{dt}(Z_{.,0}) - Z_{.,6}|^2)$ at the minimum in i_1 is $(Z_{.,5}, Z_{.,6})^T(K(\phi, \phi) + \lambda_1^{-1}I)^{-1}(Z_{.,5}, Z_{.,6})$. The proposed strategy is then to minimize (4.12) over f first and then over Z next. If discrete times $Z_{.,0}$ form a fine enough mesh of the time interval $[0, 10]$ then minimizers of $Z \rightarrow \min_f \mathcal{L}(f, Z)$ are well approximated by substituting $Z_{.,4}, Z_{.,6}, Z_{.,8}$ (which represent the values of the time derivatives of V_3, i_1 and i_2 at the discrete time points) with $Z_{.,4} = K(\phi^2, \phi^1)K(\phi^1, \phi^1)^{-1}Z_{.,3}$, $Z_{.,6} = K(\phi^2, \phi^1)K(\phi^1, \phi^1)^{-1}Z_{.,5}$ and $Z_{.,8} = K(\phi^2, \phi^1)K(\phi^1, \phi^1)^{-1}Z_{.,7}$ (which are the values of the time derivatives of V_3, i_1 and i_2 at the discrete time points obtained by simply regressing the values of V_3, i_1 and i_2). We have used this technique here and Fig. 7 shows the true and recovered values of all functions and variables of the system (in the time interval $[0, t]$ for the functions $t \rightarrow V_1, V_2, V_3, i_1, i_2, i_3$, in the range spanned by (a) i_1 for L_1 , (b) i_2 for L_2 , (c) i_3 for R , and (d) V_3 for C).

5. General solution to Computational Graph Completion problems

We will now describe the Gaussian Process (GP) framework for solving Problem 1. This framework will allow us to generalize the particular strategy used in Sec. 4.

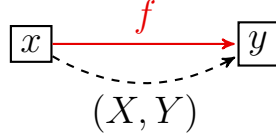
5.1. Computational Graph Completion with Gaussian Processes. Our approach to solving CGC problems can be summarized as (1) replacing unknown functions by GPs, and (2) approximating those functions by the MAP estimator of those GPs given available data. The covariance kernels of these GPs may be pre-determined by the user (based on prior information on regularity/symmetries) or learned from data (e.g., using Kernel Flows as described in [29, 13]). We will focus this manuscript on the situation where those kernels are given. We assume that the nodes of our computational graphs represent variables in separable Hilbert spaces and employ GPs with scalar/vector/operator-valued kernels as covariance kernels (see [26] for a short reminder on operator-valued kernels, their feature maps, and corresponding Gaussian Processes). If f is a function mapping the variable x to the variable y , we may not specify the (finite or infinite dimensional) Hilbert spaces \mathcal{X} and \mathcal{Y} containing x and y , nor the underlying (possibly operator valued) kernel¹ $K : \mathcal{X} \times \mathcal{X} \rightarrow \mathcal{L}(\mathcal{Y})$ used as a covariance kernel for the GP randomization of f . Indeed, one motivation for the proposed framework is to enable high-level computation and reasoning with GPs, and abstract away/automatize the underlying technicalities. Thus, prior to presenting our general solutions to Problem 1 we will first set notations by formulating and solving classical interpolation and regression problems as CGC problems with GPs.

5.2. Jointly measured/observed variables. If for some $s \in \{1, \dots, N\}$, two and only two variables $X_{s,i}$ and $X_{s,j}$ are observed then we draw a dashed arrow between nodes i and j . If $X_{s,j} = g(X_{s,i})$ where g is a known function then we may label that arrow with

¹Write $\mathcal{L}(\mathcal{Y})$ for the set of bounded linear operators mapping \mathcal{Y} to \mathcal{Y}

g (to represent the corresponding data) and point the arrow from i to j . Otherwise, we may label the dashed arrow with the corresponding data.

5.3. Interpolation. The simplest example of computation graph completion problem, illustrated in the following diagram, is that of identifying an unknown function f from data $(X_i, Y_i = f(X_i))_{i=1, \dots, N}$.



Given a kernel K , the proposed GP approach is the classical GP interpolation one of approximating f with the conditional expectation

$$f^\dagger(x) = \mathbb{E}[\xi | \xi(X) = Y] \quad (5.1)$$

where $\xi \sim \mathcal{N}(0, K)$ is a centered GP with covariance kernel K , $X = (X_1, \dots, X_N)$, $Y = (Y_1, \dots, Y_N)$ and $\xi(X) := (\xi(X_1), \dots, \xi(X_N))$. Writing \mathcal{H}_K and $\|\cdot\|_K$ for the RKHS space and norm associated with K , recall (see appendix) that f^\dagger can also be identified as the minimizer of

$$\begin{cases} \text{minimize}_{f \in \mathcal{H}_K} & \|f\|_K^2 \\ \text{s.t.} & f(X) = Y, \end{cases} \quad (5.2)$$

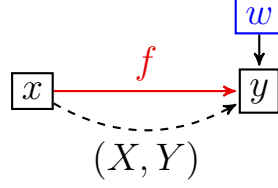
and admits the representer formula

$$f^\dagger(\cdot) = K(\cdot, X)K(X, X)^{-1}Y, \quad (5.3)$$

where $K(\cdot, X)$ is the N -vector with entries $K(\cdot, X_i)$ and $K(X, X)$ is the $N \times N$ matrix with entries $K(X_i, X_j)$.

5.4. Random variables. Variables may be primal (black square), aggregation of other variables (black circle), or random (blue square). We write \mathcal{V}_r for the set of nodes representing random variables. Using the notations of Sec. 3, we assume that the random variables $(X_{s,i})_{1 \leq s \leq N, i \in \mathcal{V}_r}$ are independent centered Gaussian random variables/vectors/fields with covariances matrices/operators $(K_i)_{i \in \mathcal{V}_r}$. Although we require independence for ease of presentation, this assumption imposes no limitation since correlations and other distributions can be considered by pushing forward Gaussian vectors through known functions.

5.5. Regression. The following diagram illustrates the computation graph completion problem of identifying an unknown function f given noisy observations $(X_i, Y_i)_{i=1, \dots, N}$ of f , where $Y_i = f(X_i) + W_i$ and the W_i are i.i.d. $\mathcal{N}(0, \sigma^2 I_{\mathcal{Y}})$ random variables. Recall that we draw random variables in blue. We will use random variables (noise) to regularize the recovery/approximation of unknown functions from data. The function associated with the arrow connecting w to y is the identity function which omit as a label to simplify the display of our diagrams.



Given a kernel K , the proposed approach is then to consider the GP $\xi \sim \mathcal{N}(0, K)$ and approximate f with the conditional expectation

$$f^\dagger(x) = \mathbb{E}[\xi | \xi(X) + W = Y] \quad (5.4)$$

where W is the N -vector with entries W_i . (5.4) can be identified as the minimizer of

$$\begin{cases} \text{minimize}_{f \in \mathcal{H}_K, W \in \mathcal{Y}^N} & \|f\|_K^2 + \frac{1}{\sigma^2} \|W\|_{\mathcal{Y}^N}^2 \\ \text{s.t.} & f(X) + W = Y, \end{cases} \quad (5.5)$$

i.e. (using the constraint to eliminate W), the minimizer of,

$$\text{minimize}_{f \in \mathcal{H}_K} \|f\|_K^2 + \frac{1}{\sigma^2} \|f(X) - Y\|_{\mathcal{Y}^N}^2, \quad (5.6)$$

which admits the following representer formula,

$$f^\dagger(x) = K(x, X)(K(X, X) + \sigma^2 I)^{-1} Y. \quad (5.7)$$

Remark 5.1. *Although this (classical) approach may appear simple, it can be highly effective when the underlying kernel is also learned from data [13, 12]. Considering the extrapolation of time series obtained from satellite data as an example, this simple data-adapted kernel perspective outperforms (both in complexity and accuracy) PDE-based and ANN-based methods [12].*

5.6. General CGC solution with GPs. Consider the general CGC problem 1. The proposed GP solution is to randomize the unknown functions $(f_e)_{e \in \mathcal{E}_u}$ with independent² centered GPs with kernels $(K_e)_{e \in \mathcal{E}_u}$ and approximate those unknown functions with a MAP estimator given the data. For $j \in \mathcal{V}$ write $X_{\cdot, j}$ for the column j of the matrix X ($(X_{s, j})_{1 \leq s \leq N}$). For a function f with domain \mathcal{X}_j write $f(X_{\cdot, j})$ for the column vector with entries $(f(X_{s, j}))_{1 \leq s \leq N}$. For $e \in \mathcal{E}$, write $a(e)$ is the node at the origin of the arrow e . For $i \in \mathcal{V}_r$ and $x_i \in \mathcal{X}_i$, write $\|x_i\|_{K_i}^2 := x_i^T K_i^{-1} x_i$ for the (RKHS) norm defined by the covariance matrix/operator K_i . Write \mathcal{V}_\square^u for the set of square nodes with at least one incoming arrow. For $e = (i, j) \in \mathcal{E}$ write f_e or $f_{i, j}$ for the function represented by e . For $j \in \mathcal{V}$, write $e \rightsquigarrow j$ for the set of arrows $e \in \mathcal{E}$ ending in j . Then the proposed GP solution to the CGC problem is to approximate the unknown functions $(f_e)_{e \in \mathcal{E}_u}$ and the matrix X with minimizers $(f_e^\dagger)_{e \in \mathcal{E}_u}$ and Z^\dagger of the variational problem.

$$\begin{cases} \text{minimize}_{(f_e)_{e \in \mathcal{E}_u}, Z, (Y_e)_{e \in \mathcal{E}}} & \sum_{e \in \mathcal{E}_u} \|f_e\|_{K_e}^2 + \sum_{s=1}^N \sum_{i \in \mathcal{V}_r} \|Z_{s, i}\|_{K_i}^2 \\ \text{s.t.} & f_e(Z_{\cdot, a(e)}) = Y_{\cdot, e}, \text{ for } e \in \mathcal{E}, \\ \text{and} & Z_{\cdot, j} = \sum_{e \rightsquigarrow j} Y_{\cdot, e}, \text{ for } j \in \mathcal{V}_\square^u, \\ \text{and} & Z_{\cdot, j} = \otimes_{i \rightsquigarrow j} Z_{\cdot, i}, \text{ for } j \in \mathcal{V}_\circ, \\ \text{and} & Z[M] = X[M]. \end{cases} \quad (5.8)$$

²Evidently, the independence assumption can be relaxed.

where the minimization is over $(f_e)_{e \in \mathcal{E}_u} \in \prod_{e \in \mathcal{E}} \mathcal{H}_{K_e}$, $Z = \{Z_{s,i} \in \mathcal{X}_i \mid 1 \leq s \leq N, i \in \mathcal{V}\}$ and $(Y_{s,e})_{1 \leq s \leq N, e \in \mathcal{E}}$ (with $Y_{s,e} \in \mathcal{R}(f_e)$, writing $\mathcal{R}(f_e)$ for range of f_e). Minimizing over $(f_e)_{e \in \mathcal{E}_u}$ first in (5.8) we obtain the following theorem turning the MAP estimation problem into a computationally tractable problem.

Theorem 5.2. $(f_e)_{e \in \mathcal{E}_u}$, Z and the $Y_{\cdot,e}$ are a minimizer of (5.8) if and only if

$$f_e(\cdot) = K_e(\cdot, Z_{\cdot,a(e)}^\dagger) K_e(Z_{\cdot,a(e)}^\dagger, Z_{\cdot,a(e)}^\dagger)^{-1} Y_e^\dagger \quad (5.9)$$

where $(Y_e^\dagger)_{e \in \mathcal{E}}$ and Z^\dagger are a minimizer of

$$\begin{cases} \text{minimize}_{Z, (Y_e)_{e \in \mathcal{E}_u}} & \sum_{e \in \mathcal{E}_u} Y_e^T K_e(Z_{\cdot,a(e)}, Z_{\cdot,a(e)})^{-1} Y_e + \sum_{s=1}^N \sum_{i \in \mathcal{V}_r} \|Z_{s,i}\|_{K_i}^2 \\ \text{s.t.} & f_e(Z_{\cdot,a(e)}) = Y_{\cdot,e}, \text{ for } e \in \mathcal{E}/\mathcal{E}_u, \\ \text{and} & Z_{\cdot,j} = \sum_{e \rightsquigarrow j} Y_{\cdot,e}, \text{ for } j \in \mathcal{V}_\square, \\ \text{and} & Z_{\cdot,j} = \otimes_{i \rightsquigarrow j} Z_{\cdot,i}, \text{ for } j \in \mathcal{V}_\circ, \\ \text{and} & Z[M] = X[M]. \end{cases} \quad (5.10)$$

5.7. Optimal recovery and gamblets. Consider a separable Banach space of functions \mathcal{B} and its dual \mathcal{B}^* with their duality pairing denoted by $[\cdot, \cdot]$. If \mathcal{B} is a space of functions $u : \mathcal{X} \rightarrow \mathcal{Y}$ then each element of \mathcal{B} can be extended to a linear functional mapping $\phi \in \mathcal{B}^*$ to $[\phi, u] \in \mathbb{R}$. This simple observation leads to a generalization of CGC to computational graphs with variables in \mathcal{B}^* . To that end consider the problem, illustrated in the following diagram, of recovering an unknown element $u \in \mathcal{B}$ (seen as a function mapping $\phi \in \mathcal{B}^*$ to $u(\phi) := [\phi, u] \in \mathbb{R}$) given the observation of $(Y_i := [\phi_i, u])_{i=1, \dots, N} \in \mathbb{R}^N$ where the ϕ_i are N linearly independent elements of \mathcal{B}^* .

$$\begin{array}{ccc} \boxed{\varphi} & \xrightarrow{u} & \boxed{[\varphi, f]} \\ & \text{---} & \\ & (\phi, Y) & \end{array} \quad (5.11)$$

To define the proposed GP solution to this CGC problem, we introduce a covariance operator [27, Chap. 11] defined as a linear bijection $K : \mathcal{B}^* \rightarrow \mathcal{B}$ that is symmetric ($[\phi, K\varphi] = [\varphi, K\phi]$) and positive ($[\phi, K\phi] > 0$ for $\phi \neq 0$). If the elements of \mathcal{B} are continuous functions then, for ease of notations, we also write $K(x, x') := [\delta_x, K\delta_{x'}]$ for the kernel associated with K . Consider the GP $\xi \sim \mathcal{N}(0, K)$ defined ([27, Chap. 17] and [25, Sec. 8]) as an isometry from \mathcal{B}^* to a Gaussian space mapping each $\varphi \in \mathcal{B}^*$ to a centered scalar valued Gaussian random variable with variance $[\varphi, K\varphi]$. The GP solution to this CGC problem is then to approximate f with the conditional expectation (writing $\xi(\phi)$ for the vector with entries $\xi(\phi_i)$)

$$u^\dagger = \mathbb{E}[\xi | \xi(\phi) = Y]. \quad (5.12)$$

Writing $\|u\|_K^2 := [K^{-1}u, u]$ for the quadratic norm defined by K on \mathcal{B} , u^\dagger can also be identified as the minimizer of (writing $u(\phi)$ for the vector with entries $[\phi_i, u]$)

$$\begin{cases} \text{minimize}_{u \in \mathcal{B}} & \|u\|_K^2 \\ \text{s.t.} & u(\phi) = Y, \end{cases} \quad (5.13)$$

and admits the representer formula

$$[\varphi, u^\dagger] = K(\varphi, \phi)K(\phi, \phi)^{-1}K\phi \quad (5.14)$$

where $K\phi$ is the N -vector with entries $K\phi_i$, $K(\phi, \phi)$ is the $N \times N$ matrix with entries $[\phi_i, K\phi_j]$ and $K(\varphi, \phi)$ is the N -vector with entries $[\varphi, K\phi_i]$.

Remark 5.3. A particular case of the example considered here is $\mathcal{B} = \mathcal{H}_0^s(\Omega)$ (writing $H_0^s(\Omega)$ for the closure of the set of smooth functions with compact support in Ω with respect to the Sobolev norm $\|\cdot\|_{H^s(\Omega)}$), with its dual $\mathcal{B}^* = H^{-s}(\Omega)$ defined by the pairing $[\phi, v] := \int_{\Omega} \phi v$ obtained from the Gelfand triple $H^s(\Omega) \subset L^2(\Omega) \subset H^{-s}(\Omega)$ [27, Chap. 2]. Given an elliptic operator $\mathcal{L} : H_0^s(\Omega) \rightarrow H^{-s}(\Omega)$ (i.e., a linear bijection that is positive and symmetric in the sense that $\int_{\Omega} u\mathcal{L}u \geq 0$ and $\int_{\Omega} u\mathcal{L}v = \int_{\Omega} v\mathcal{L}u$) let K be the solution map \mathcal{L}^{-1} . Let the ϕ_i be (1) (for $s > d/2$) delta Dirac functions δ_{x_i} centered at N homogeneously distributed points x_i of Ω , or (2) (for $s > 0$) indicator functions of subsets τ_i forming a regular partition of Ω [27, Sec. 4.3]. Then the minimizer of (5.13) is

$$u^\dagger = \sum_{i=1}^n [\phi_i, u] \psi_i \quad (5.15)$$

where the elements $\psi_i \in \mathcal{B}$ (defined by $\psi_i = \sum_{j=1}^N K(\phi, \phi)_{i,j}^{-1} K\phi_j$) are optimal recovery splines [19] or gamblets [23, 24] adapted to the operator \mathcal{L} (i.e., operator adapted wavelets [27] that are both localized and near optimal in approximating the solution space $\mathcal{L}^{-1}L^2(\Omega)$). We refer to [27, 22] for a further survey of interplays between numerical approximation and statistical inference.

5.8. Computational Graph Completion with generalized variables. The setting of Sec. 5.7 allows us to generalize CGC to situations where some of the variables x_i are vectors whose entries are linear functionals action on spaces of functions, i.e. $\mathcal{X}_i = (\mathcal{B}_e^*)^m$ where e is an edge originating from i , \mathcal{B}_e^* is the dual space of space of functions, e is representing an element of $f_e \in \mathcal{B}_e$ and, for $x_i = (x_{i,1}, \dots, x_{i,m})$, $f_e(x_i)$ is interpreted as the vector $([x_{i,1}, f_e], \dots, [x_{i,m}, f_e])$. In that situation, the results and formulas of Sec. 5.6 hold true with the following alterations: if f_e is unknown and acting on linear functionals, then the K_e describing its GP randomization is a covariance operator and for $x_i, x'_i \in (\mathcal{B}_e^*)^m$, $K_e(x_i, x'_i)$ is a matrix with entries $[x_{i,j}, K_e x'_{i,l}]$. In that setting an unknown function mapping x to $(u(x), \Delta u(x))$ should be displayed as

$$\boxed{x} \longrightarrow \boxed{(\delta_x, -\delta_x \circ \Delta)} \xrightarrow{u} \boxed{(u(x), -\Delta u(x))}$$

but for ease of presentation, we will simplify such diagrams by drawing them as follows.

$$\boxed{x} \xrightarrow{u} \boxed{(u(x), -\Delta u(x))}$$

5.9. Relaxation and regularization with random variables. A particular case of the solution presented in Sec. 5.6 and 5.8 is to use random variables to regularize the underlying constraints imposed by unknown functions, known functions, and measurements. As shown in [25] (see also Sec. 6.4), from the perspective of kriging with composed GPs/kernels, relaxing output constraints with nuggets (small Gaussian noise capturing the variability of the data [8]) is not sufficient to ensure stability, one must also relax

all composition steps³. To describe this consider (for ease of presentation) Problem 1 in the setting where there are no random variables $\mathcal{V}_r = \emptyset$. Let $f := (f_e)_{e \in \mathcal{E}_u}$ represent all unknown functions and let $g := (g_e)_{e \in \mathcal{E}/\mathcal{E}_u}$ represent all known functions. Then, given strictly positive relaxation parameters $\lambda_{i,j} > 0$ (described below), the proposed solution to Problem 1 is to recover f and X with a minimizer of the following variational problem

$$\begin{cases} \text{minimize}_{f,Z,Y} & \|f\|^2 + \mathcal{L}_1(f, Y, Z) + \mathcal{L}_2(Y, Z) + \mathcal{L}_3(Z[M], X[M]), \\ \text{s.t.} & Z_{\cdot,j} = \otimes_{i \rightsquigarrow j} Z_{\cdot,i}, \text{ for } j \in \mathcal{V}_\circ. \end{cases} \quad (5.16)$$

where $\|f\|^2 := \sum_{e \in \mathcal{E}_u} \|f_e\|_{K_e}^2$ is the sum of the RKHS norms of all unknown functions,

$$\mathcal{L}_1(f, Z) := \sum_{e \in \mathcal{E}} \lambda_{1,b(e)} \|f_e(Z_{\cdot,a(e)}) - Y_e\|_{\mathcal{X}_{b(e)}^N}^2, \quad (5.17)$$

relaxes dependencies between known and unknown functions, Y and Z ,

$$\mathcal{L}_2(Z, Y) := \sum_{j \in \mathcal{V}_\circ^i} \lambda_{2,j} \|Z_{\cdot,j} - \sum_{e \rightsquigarrow j} Y_e\|_{\mathcal{X}_j^N}^2, \quad (5.18)$$

relaxes dependencies between Y and Z , and

$$\mathcal{L}_3(Z[M], X[M]) := \sum_{i | M_{s,i}=1} \lambda_{3,i} \|Z_{\cdot,i} - X_{\cdot,i}\|_{\mathcal{X}_i^N}^2 \quad (5.19)$$

relaxes measurement/data constraints. Minimizing over f first in (5.16) we obtain the following theorem.

Theorem 5.4. *f, Y and Z are a minimizer of (5.16) if and only if, for $f_e \in \mathcal{E}_u$,*

$$f_e(\cdot) = K_e(\cdot, Z_{\cdot,a(e)}^\dagger) (K_e(Z_{\cdot,a(e)}^\dagger, Z_{\cdot,a(e)}) + \lambda_{1,a(e)}^\dagger I)^{-1} Y_e^\dagger \quad (5.20)$$

where Y^\dagger and Z^\dagger are a minimizer of

$$\begin{cases} \text{minimize}_{Z,Y} & \sum_{e \in \mathcal{E}_u} Y_e^T (K_e(Z_{\cdot,a(e)}, Z_{\cdot,a(e)}) + \lambda_{1,a(e)} I)^{-1} Y_e \\ & + \sum_{e \in \mathcal{E}/\mathcal{E}_u} \lambda_{1,b(e)} \|f_e(Z_{\cdot,a(e)}) - Y_e\|_{\mathcal{X}_{b(e)}^N}^2 \\ & + \mathcal{L}_2(Y, Z) + \mathcal{L}_3(Z[M], X[M]), \\ \text{s.t.} & Z_{\cdot,j} = \otimes_{i \rightsquigarrow j} Z_{\cdot,i}, \text{ for } j \in \mathcal{V}_\circ. \end{cases} \quad (5.21)$$

Note that the proposed relaxation is equivalent to the CGC solution (5.8) with a modification of the underlying computational graph corresponding to the addition of independent centered Gaussian random variable with covariance matrices/operators (1) $I_{\mathcal{X}_{b(e)}}/\lambda_{1,b(e)}$ to the output of each function f_e , (2) $I_{\mathcal{X}_j}/\lambda_{2,j}$ to each node $j \in \mathcal{V}_\circ^i$, (3) $I_{\mathcal{X}_j}/\lambda_{3,j}$ to each measurement of $X_{s,j}$.

³This type of regularization was introduced in [25] (as a principled and rigorous alternative to Dropout [35]) for ANNs/ResNets and their kernelized variants where it was shown to be necessary and sufficient to avoid regression instabilities (the lack of stability/continuity of regressors with respect to data and input variables).

5.10. Feature maps and Artificial Neural Networks. In the setting of Sec. 5.9, write ψ_e and \mathcal{F}_e for the feature map and space associated with the kernel K_e , i.e. ψ_e maps $\mathcal{X}_{a(e)}$ to the space of bounded linear operators from $\mathcal{X}_{b(e)}$ to \mathcal{F}_e , and $y^T K_e(z, z') y' = \langle \psi_e(z) y, \psi_e(z') y' \rangle_{\mathcal{F}_e}$ for $(x, x', y, y') \in \mathcal{X}_{a(e)}^2 \times \mathcal{X}_{b(e)}^2$, which we write as $K_e(z, z') = \psi_e^T(z') \psi_e(z)$. When the \mathcal{F}_e are finite-dimensional then an alternative approach is to represent the unknown functions as $f_e = \psi_e^T \alpha_e$ where the α_e are feature map coefficients determined by minimizing (5.16) over the α_e and Z, Y with

$$\|f\|^2 := \sum_{e \in \mathcal{E}_u} \|\alpha_e\|_{\mathcal{F}_e}^2 \quad (5.22)$$

and

$$\mathcal{L}_1(f, Z) := \sum_{e \in \mathcal{E}} \lambda_{1,b(e)} \|\psi_e^T(Z_{\cdot, a(e)}) \alpha_e - Y_e\|_{\mathcal{X}_{b(e)}^N}^2. \quad (5.23)$$

If the feature maps ψ_e themselves are parameterized by hyperparameters θ_e then those hyperparameters can also be learned from data via MAP estimation (as in [25]), Kernels Flows [29, 5] or MLE [5]. By interpreting ANNs as a particular case of parameterized feature map [38, 25] kernel learning techniques could be employed to solve CGC problems with ANNs. Note that replacing unknown functions with ANNs is equivalent to replacing unknown functions with sub-graphs whose unknown functions are parameterized by the layers of the network (see Sec. 6.3). Furthermore when applied to solving/learning PDEs (Sec. 6.1 and 6.1), and compared to prototypical ANN-based approaches (such as PINNs [31]), the loss (5.16) includes a RKHS regularization term on unknown functions and the relaxation of all composition steps, which are essential for the convergence and stability of the proposed method. We will not develop further the ANN-based approach to CGC in this paper and refer to remarks 5.1 and 6.1 for motivations for its focus on GPs/kernel methods.

6. Further examples

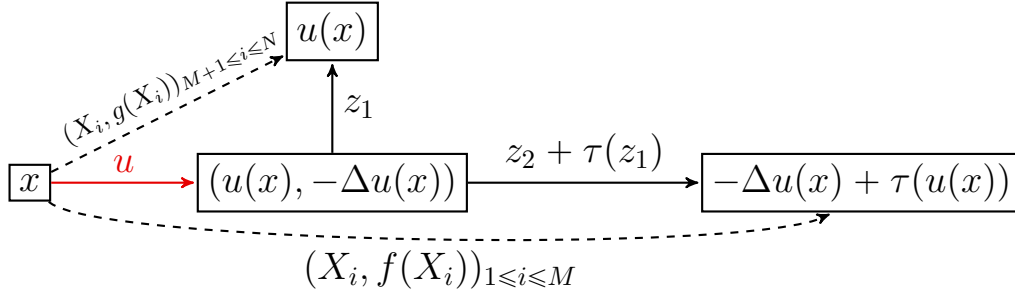
We will now illustrate the flexibility and scope of the CGC framework through examples. These examples include the seamless CGC representation of known methods and the discovery of new ones.

6.1. Solving nonlinear PDEs. We will now show that GP approach to solving nonlinear PDEs, introduced in [4], can naturally be represented as a CGC solution. As in [4] the nonlinear PDE can be arbitrary but, for ease of presentation, we will only consider the following prototypical nonlinear elliptic PDE [4, Sec. 1.1]

$$\begin{cases} -\Delta u(x) + \tau(u(x)) = f(x), & \forall x \in \Omega, \\ u(x) = g(x), & \forall x \in \partial\Omega, \end{cases} \quad (6.1)$$

where τ is a nonlinearity (e.g., $\tau(u) = u^3$) and $\Omega \subset \mathbb{R}^d$ and τ, f, g are continuous and such that (6.1) admits a unique strong solution in $H^s(\Omega)$ with $s > d/2 + 2$ (so that u has continuous C^2 derivatives). To approximate the solution of (6.1) as a CGC problem, let X_1, \dots, X_M and X_{M+1}, \dots, X_N be a finite number of collocation points on Ω and $\partial\Omega$. Then, as illustrated in the following diagram, consider the problem of approximating the unknown function u given $u(X_i) = g(X_i)$ for $i = M + 1, \dots, N$ and

$$(-\Delta u + \tau(u))(X_i) = f(X_i) \text{ for } i = 1, \dots, M.$$



Note that we are using the setting of Sec. 5.8. Replacing u with a centered GP $\xi \sim \mathcal{N}(0, K)$ with kernel $K : \Omega \times \Omega \rightarrow \mathbb{R}$ (chosen so that $\mathcal{H}_K \subset C^2(\Omega) \cap C(\bar{\Omega})$), we recover the solution introduced in [4]. As detailed in [4], this solution is to approximate u with the MAP estimator of ξ given the data (given $\xi(X_i) = g(X_i)$ for $i = M + 1, \dots, N$ and $-(\Delta \xi + \tau(\xi))(X_i) = f(X_i)$ for $i = 1, \dots, N$), which can be computed as a minimizer of

$$\begin{cases} \text{minimize} & \begin{cases} \text{minimize}_u & \|u\| \\ \text{s.t.} & u(X_i) = z_i^{(1)} \text{ and } -\Delta u(x_i) = z_i^{(2)}, \text{ for } i = 1, \dots, M, \end{cases} \\ \text{s.t.} & \begin{cases} z_i^{(2)} + \tau(z_i^{(1)}) = f(X_i), & \text{for } i = 1, \dots, M, \\ z_i^{(1)} = g(X_i), & \text{for } i = M + 1, \dots, N, \end{cases} \end{cases} \quad (6.2)$$

where the intermediate variables $z_i^{(1)} := u(X_i)$ and $z_i^{(2)} := \Delta u(X_i)$ appear as nodes in the computational graph. After reduction, (6.2) can then be solved using a variant of the Gauss-Newton algorithm [4], which implies that the complexity of the method inherits that of the state-of-the-art solvers for inverting/compressing dense kernel matrices (e.g., in $N \log^{2d} N$ complexity with a variant of [33]). Furthermore, [4] also shows that if the kernel K is adapted in the sense that $u \in \mathcal{H}_K$ and $\mathcal{H}_K \subseteq H^s(\Omega)$ for some $s > 2 + d/2$, then the proposed approach is guaranteed to converge (pointwise and in $\mathcal{H}^t(\Omega)$ for $t < s$) as the fill distance between collocation points goes to zero [4, Thm. 1.2].

Remark 6.1. *Current learning methods for scientific computing can be divided into two main categories: (1) methods based on variants of artificial neural networks (ANNs) with Physics Informed Neural Networks as a prototypical example [31]; and (2) methods based on kernels and Gaussian Processes (GPs) [37, 34, 22, 15, 30, 6] with gamblers [23, 24, 27] as a prototypical example. Methods of type (2) were essentially limited to linear/quasi-linear/time-dependent PDEs, and they have been recently generalized to arbitrary non-linear PDEs [4]. As discussed in [4], methods of type (2) hold potential for considerable advantages over methods of type (1), in terms of theoretical analysis, numerical implementation, regularization, guaranteed convergence, automatization, interpretability, and higher-level reasoning. Furthermore, by interpreting ANNs as data-dependent feature maps, methods of type (1) can be analyzed, generalized, and regularized as methods of type (2) with data adapted kernels [25, 2].*

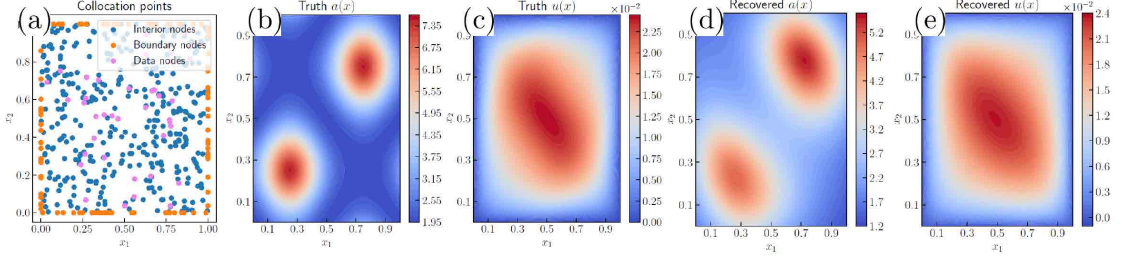
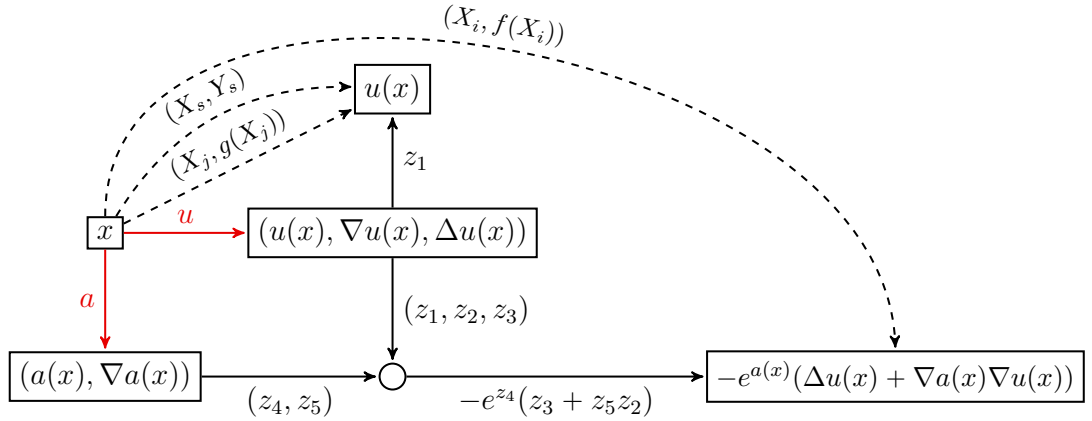


FIGURE 8. [4, Fig. 5]. (a) Collocation and data points; (b) true a ; (c) true u ; (d) recovered a ; (e) recovered u .

6.2. Learning PDEs. In our next example we will show that GP approach to learning PDEs, introduced in [4], can also be formulated as a CGC solution. The PDE can be nonlinear and arbitrary but, for ease of presentation, but we will only consider the prototypical inverse problem [4, Sec. 4] of approximating the coefficient a and the solution u of the following PDE ($\Omega = (0, 1)^2$)

$$\begin{cases} -\operatorname{div}(\exp(a)\nabla u)(x) = f(x), & x \in \Omega, \\ u(x) = g, & x \in \partial\Omega. \end{cases} \quad (6.3)$$

given the observation of the value Y_i of u at a finite number of collocation points X_j . Consider the following CGC diagram above and recover a , u from the measurements $u(X_i) = Y_i$ at a finite number of data points X_i (colored in magenta in Fig. 8.(a)) and of the values of $-\operatorname{div}(\exp(a)\nabla u)(X_s) = f(X_s)$ and $u(X_j) = g(X_j)$ at a finite number of collocation points $X_s \in \Omega$ and $X_j \in \partial\Omega$.



The GP solution to this CGC problem recovers that of [4, Sec. 4] illustrated in Fig. 8. Given two kernels Γ and K (such that \mathcal{H}_Γ and \mathcal{H}_K contain C^1 and C^2 functions), this

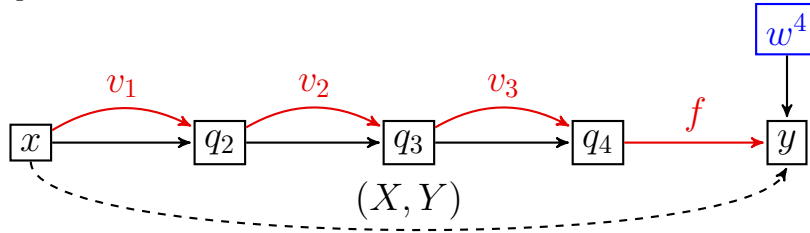
solution is to identify a and u as minimizers of

$$\left\{ \begin{array}{l} \text{minimize}_{u,a,z^{(1)},\dots,z^{(5)}} \|u\|_K^2 + \|a\|_\Gamma^2 \\ \text{s.t. } \Delta u(X_i) = (z_i^{(3)}, \nabla u(X_i) = z_i^{(2)}, a(X_i) = z_i^{(4)}, \nabla a(X_i) = z_i^{(5)}, \text{ for } i = 1, \dots, M, \\ u(X_j) = z^{(1)}, \text{ for } j = M + 1, \dots, N, \\ u(X_s) = Y_s \text{ for } s = N + 1, \dots, N + D, \\ -e_i^{z_i^{(4)}}(z_i^{(3)} + z_i^{(5)} z_i^{(2)})(X_i) = f(X_i), \text{ for } i = 1, \dots, M, \\ z^{(1)} = g(X_j), \text{ for } j = M + 1, \dots, N, \\ z^{(1)} = Y_s \text{ for } s = N + 1, \dots, N + D. \end{array} \right. \quad (6.4)$$

6.3. ResNet and idea registration. Training ANNs can naturally be formulated as a particular case of CGC. In this example, taken from [25], we consider the problem of regressing the data $(X_i, Y_i)_{i=1}^N$ with a function of the form

$$f \circ \phi_L \text{ where } \phi_L = (I + v_L) \circ \dots \circ (I + v_1), \quad (6.5)$$

where f, v_1, \dots, v_L are unknown functions and I is the identity function. Introducing the intermediate variables $q_1 = x + v_1(x)$, $q_2 = q_1 + v_2(q_1)$ and $q_3 = q_2 + v_3(q_2)$, this nonlinear regression problem can be formulated as the CGC problem illustrated by the following graph for $L = 3$.



Given kernels Γ and K , f and the v_i can be identified as minimizers of

$$\min_{f,v_1,\dots,v_L} \frac{\nu L}{2} \sum_{s=1}^L \|v_s\|_\Gamma^2 + \lambda \|f\|_K^2 + \|f \circ \phi_L(X) - Y\|_{\mathcal{Y}^N}^2, \quad (6.6)$$

over $f \in \mathcal{H}_K$ and $v_i \in \mathcal{H}_\Gamma$. As noted in [25], if Γ and K are affine scalar operator valued kernels (of the form $\Gamma(x, x') = ((\mathbf{a})(\mathbf{x})\mathbf{a}(\mathbf{x}') + \mathbf{1})\mathbf{I}_\mathcal{X}$ and $K(x, x') = ((\mathbf{a})(\mathbf{x})\mathbf{a}(\mathbf{x}') + \mathbf{1})\mathbf{I}_\mathcal{Y}$ where \mathbf{a} is an activation function defined as an elementwise nonlinearity), then $f \circ \phi_L$ has the structure of one ResNet block [14] and minimizing (6.6) is equivalent to training that network with L_2 regularization on weights and biases.

Letting $q^1 := X$, and introducing the intermediate variables $q^{s+1} = q^s + v_s(q^s)$ for $1 \leq s \leq L$ we obtain that (f, v_1, \dots, v_L) is a minimizer of (6.6) if and only if

$$v_s(x) = \Gamma(x, q^s)\Gamma(q^s, q^s)^{-1}(q^{s+1} - q^s) \text{ for } x \in \mathcal{X}, s \in \{1, \dots, L\}, \quad (6.7)$$

and

$$f(x) = K(x, q^{L+1})(K(q^{L+1}, q^{L+1}) + \lambda^{-1}I)^{-1}Y \quad (6.8)$$

where $q^1, \dots, q^{L+1} \in \mathcal{X}^N$ is a minimizer of (write $\Delta t := 1/L$) the discrete least action principle

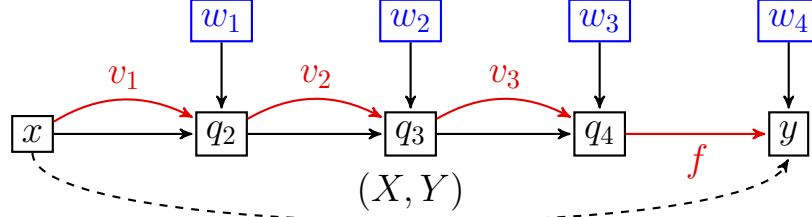
$$\begin{cases} \text{Minimize} & \frac{\nu}{2} \sum_{s=1}^L \left(\frac{q^{s+1} - q^s}{\Delta t} \right)^T \Gamma(q^s, q^s)^{-1} \left(\frac{q^{s+1} - q^s}{\Delta t} \right) \Delta t + \lambda Y^T (K(q^{L+1}, q^{L+1} + \lambda^{-1}I)^{-1} Y \\ \text{over} & q^2, \dots, q^{L+1} \in \mathcal{X}^N \text{ with } q^1 = X. \end{cases} \quad (6.9)$$

Furthermore, as $L \rightarrow \infty$, [25] establishes the convergence of the trajectory formed by the q^s towards a continuous least action principle and deduces the convergence of $f \circ \phi_L$ towards $f \circ \phi^v(\cdot, 1)$ where $\phi^v(\cdot, t)$ is the flow map of the vector field v ($\phi(x, 0) = x$ and $\dot{\phi}(x, t) = v(\phi(x, t), t)$), and (f, v) are identified as a minimizer of the following variational problem

$$\min_{f, v} \frac{\nu}{2} \int_0^1 \|v(x, t)\|_{\Gamma}^2 + \lambda \|f\|_K^2 + \|f \circ \phi(X, 1) - Y\|_{Y_N}^2. \quad (6.10)$$

(6.10), which has the structure of variational formulations used in computational anatomy [11], image registration [3] and shape analysis [39], can be seen as a generalization of image registration problem with images replaced by high dimensional shapes/forms (ideas).

6.4. Regularized ResNet. The regressor $f \circ \phi_L$ obtained in (6.3) is not continuous with respect to the data (X, Y) and unstable with respect to the input variable x [25]. A natural and rigorous approach to its regularization (which ensures the continuity and stability of the regressor), presented in [25], is to add random (noise) variables w_i to intermediate variables, as illustrated in the following diagram for $L = 3$.



With this modification (f, v_1, \dots, v_L) is then identified as a minimizers of

$$\begin{cases} \text{Minimize} & \frac{\nu}{2} L \sum_{s=1}^L (\|v_s\|_{\Gamma}^2 + \frac{1}{r} \|q^{s+1} - (I + v_s)(q^s)\|_{\mathcal{X}^N}^2) \\ & + \lambda \|f\|_{\mathcal{H}}^2 + \|f(q^{L+1}) - Y\|_{Y_N}^2 \\ \text{over} & v_1, \dots, v_L \in \mathcal{H}_{\Gamma}, f \in \mathcal{H}_K, q^1, \dots, q^{L+1} \in \mathcal{X}^N, q^1 = X, \end{cases} \quad (6.11)$$

Furthermore, (v_1, \dots, v_L, f) , is a minimizer of (6.11) if and only if $f = (6.8)$ and

$$v_s(x) = \Gamma(x, q^s) (\Gamma(q^s, q^s) + rI)^{-1} (q^{s+1} - q^s) \text{ for } x \in \mathcal{X}, s \in \{1, \dots, L\}, \quad (6.12)$$

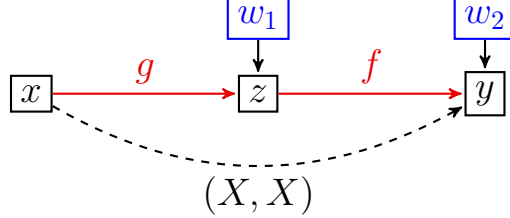
where $q^1, \dots, q^{L+1} \in \mathcal{X}^N$ is a minimizer of (write $\Delta t := 1/L$)

$$\begin{cases} \text{Minimize} & \frac{\nu}{2} \sum_{s=1}^L \left(\frac{q^{s+1} - q^s}{\Delta t} \right)^T (\Gamma(q^s, q^s) + rI)^{-1} \left(\frac{q^{s+1} - q^s}{\Delta t} \right) \Delta t \\ & + \lambda Y^T (K(q^{L+1}, q^{L+1} + \lambda^{-1}I)^{-1} Y \\ \text{over} & q^2, \dots, q^{L+1} \in \mathcal{X}^N \text{ with } q^1 = X, \end{cases} \quad (6.13)$$

The regularization process illustrated here is generic and, as discussed in Sec. 5.9, can be extended to all CGC problems by adding noise variables (acting as nuggets in the setting of kriging) to all intermediate variables.

6.5. Dimension reduction. We will now present several variants of dimension reduction methods identified as solutions of CGC problems.

6.5.1. Kernel variant of autoencoders. Consider the following diagram.



In that diagram we consider the problem of recovering two unknown functions f and g given the data $(X_i = f(g(X_i) + W_{1,i}) + W_{2,i})_{i=1,\dots,N}$, where the $W_{1,i}$ and $W_{2,i}$ are i.i.d. $\mathcal{N}(0, \sigma_1^2)$ and $\mathcal{N}(0, \sigma_2^2)$ random variables. Writing $\dim(x)$ for the dimension of the variable x , we select $\dim(x) = \dim(y) > \dim(z)$, so that the intermediate z variables act as reduced/coarse/latent variables. Writing \mathcal{X} for the domain of x and y and \mathcal{Z} for the domain of z , given two kernels $\Gamma : \mathcal{X} \times \mathcal{X} \rightarrow \mathcal{L}(\mathcal{Z})$ and $K : \mathcal{Z} \times \mathcal{Z} \rightarrow \mathcal{L}(\mathcal{X})$, the proposed GP approach is to consider the GPs $\xi_1 \sim \mathcal{N}(0, \Gamma)$ and $\xi_2 \sim \mathcal{N}(0, K)$ and approximate (g, f) with a MAP estimator of (ξ_1, ξ_2) given $(X = \xi_2(\xi_1(X) + W_1) + W_2)$. Introducing $Z = g(X) + W_1$ as an intermediate variable, these MAP estimators can be identified as minimizers of,

$$\underset{f \in \mathcal{H}_K, g \in \mathcal{H}_\Gamma, Z \in \mathcal{Z}^N}{\text{minimize}} \|g\|_\Gamma^2 + \|f\|_K^2 + \frac{1}{\sigma_2^2} \|g(X) - Z\|_{\mathcal{Z}^N}^2 + \frac{1}{\sigma_1^2} \|f(Z) - X\|_{\mathcal{X}^N}^2. \quad (6.14)$$

Following [25] we minimize over f and g first and obtain that

$$f^\dagger(x) = K(x, Z^\dagger)(K(Z^\dagger, Z^\dagger) + \sigma_2^2 I)^{-1} X, \quad (6.15)$$

and

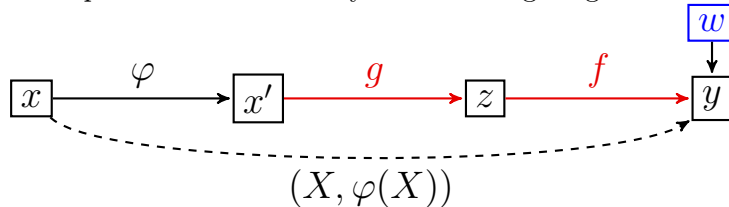
$$g^\dagger(x) = \Gamma(x, X)(\Gamma(X, X) + \sigma_1^2 I)^{-1} Z^\dagger, \quad (6.16)$$

where Z^\dagger is a minimizer of

$$\underset{Z \in \mathcal{Z}^N}{\text{minimize}} Z^T (\Gamma(X, X) + \sigma_1^2 I)^{-1} Z + X^T (K(Z, Z) + \sigma_2^2 I)^{-1} X. \quad (6.17)$$

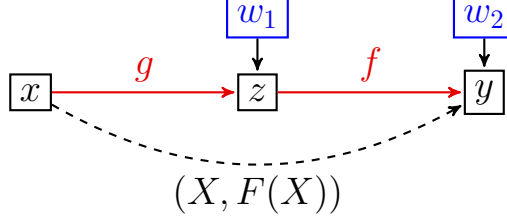
Note that if f and g are replaced by ANNs, then $f \circ g$ has the structure of an autoencoder [1]. Furthermore, if one selects K and Γ to be linear kernels (i.e., having linear feature maps) and $\sigma_1 = 0$, then one rediscovers SVD/PCA [10] as the solution of the proposed CGC problem.

6.5.2. Kernel PCA. In the following example we reformulate Kernel PCA [20] as the solution of the CGC problem illustrated by the following diagram.



This is done by interpreting φ as the feature map of a given kernel, selecting $\dim(x') = \dim(y) > \dim(z)$, and recovering f and g with linear kernels.

6.5.3. Nonlinear active subspace. We now present a generalization of active subspace methods [7] to nonlinear spaces. Consider the following diagram.



In that diagram $F : \mathcal{X} \rightarrow \mathcal{Y}$ is a computable function and we seek to reduce its dimension by selecting $\dim(z) < \min(\dim(x), \dim(y))$ and approximating F with $f \circ g$. Given $(X, F(X))$, where X is a set of points in the input space, and given two kernels K and Γ , the proposed CGC solution is to obtain (f, g) as minimizer of

$$\underset{f \in \mathcal{H}_K, g \in \mathcal{H}_\Gamma, Z \in \mathcal{Z}^N}{\text{minimize}} \|g\|_\Gamma^2 + \|f\|_K^2 + \frac{1}{\sigma_1^2} \|g(X) - Z\|_{\mathcal{Z}^N}^2 + \frac{1}{\sigma_2^2} \|f(Z) - F(X)\|_{\mathcal{Y}^N}^2. \quad (6.18)$$

which is a simple variant of (6.14), whose minimizers are of the form

$$f^\dagger(x) = K(x, Z^\dagger)(K(Z^\dagger, Z^\dagger) + \sigma_2^2 I)^{-1} F(X), \quad (6.19)$$

and

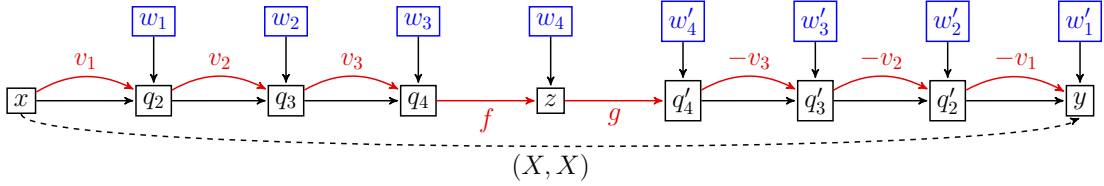
$$g^\dagger(x) = \Gamma(x, X)(\Gamma(X, X) + \sigma_1^2 I)^{-1} Z^\dagger, \quad (6.20)$$

where Z^\dagger is a minimizer of

$$\underset{Z \in \mathcal{Z}^N}{\text{minimize}} Z^T (\Gamma(X, X) + \sigma_1^2 I)^{-1} Z + F(X)^T (K(Z, Z) + \sigma_2^2 I)^{-1} F(X). \quad (6.21)$$

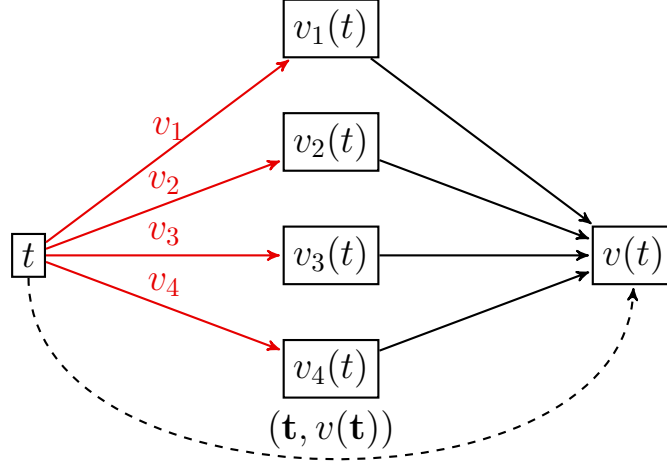
Note that if f and g are replaced by linear maps and if F is linear then (for $\sigma_1 = 0$) one rediscovers the SVD approximation of F .

6.5.4. Nonlinear PCA variant. We now present a dimension reduction variant obtaining by combining the diagrams of subsections 6.5 and 6.4.



Select $\dim(x) = \dim(y)$, $\dim(z) < \dim(x)$ and let the kernels associated with f and g be linear kernels. Then the proposed approach seeks to learn a deformation $\phi_L = (I + v_L) \circ \dots \circ (I + v_1)$ of the input space such that linear SVD performs well on that input space. Note that the second portion of the diagram corresponds to the map $(I - v_1) \circ \dots \circ (I - v_L)$ which is an approximation of the inverse of ϕ_L (and an exact inverse in the limit $L \rightarrow \infty$).

6.6. Mode decomposition. This example is taken from [28]. Let v_1, \dots, v_m be unknown functions mapping $[0, 1]$ to \mathbb{R} . Consider the problem of recovering v_1, \dots, v_m given the observation of $v := v_1 + \dots + v_m$ at $\mathbf{t} := (t_1, \dots, t_N) \in [0, 1]^N$. This mode decomposition problem can naturally be formulated as the CGC problem illustrated in the following diagram for $m = 4$.



Given kernels K_1, \dots, K_m , the GP solution is then to recover v_1, \dots, v_m with the minimizer of

$$\begin{cases} \text{minimize}_{v_1, \dots, v_m} & \sum_{i=1}^m \|v_i\|_{K_i}^2 \\ \text{s.t.} & \sum_{i=1}^m v_i(\mathbf{t}) = v(\mathbf{t}). \end{cases} \quad (6.22)$$

Writing $K := \sum_{i=1}^m K_i$ and w_i for the minimizer over v_i of (6.22), we have

$$w_i(t) = K_i(t, \mathbf{t})K(\mathbf{t}, \mathbf{t})^{-1}v(\mathbf{t}). \quad (6.23)$$

Evidently, the selection of the kernels K_i depends on prior information on the modes v_i . For instance, consider the case where, $m = 4$, $v_1(t) = a_1(t) \cos(\theta_1(t)) + b_1(t) \sin(\theta_1(t))$, $v_2(t) = a_2(t) \cos(\theta_2(t)) + b_2(t) \sin(\theta_2(t))$, $v_3(t) = a_3(t)$, v_4 is white-noise, the a_i and b_i are unknown smooth functions and the θ_i are known. Replacing a_1, b_1, a_2, b_2 by independent centered GPs with Gaussian kernel $e^{-\frac{(s-t)^2}{\gamma^2}}$ results in the selection

$$K_1(s, t) = e^{-\frac{(s-t)^2}{\gamma^2}} (\cos(\theta_1(s)) \cos(\theta_1(t)) + \sin(\theta_1(s)) \sin(\theta_1(t))) \quad (6.24)$$

and

$$K_2(s, t) = e^{-\frac{(s-t)^2}{\gamma^2}} (\cos(\theta_2(s)) \cos(\theta_2(t)) + \sin(\theta_2(s)) \sin(\theta_2(t))). \quad (6.25)$$

For v_3 we select $K_3(s, t) = 1 + st + e^{-\frac{(s-t)^2}{4}}$. Finally since v_4 is white noise we use $K_4(s, t) = \delta(s - t)$. Fig. 9 illustrates the proposed approach (\mathbf{t} corresponds to 320 points distributed over a grid of $[0, 1]$). Note that the selection of K_1 and K_2 can also be formalized by unpacking v_1 and v_2 into subgraphs (illustrated below for v_1) involving the

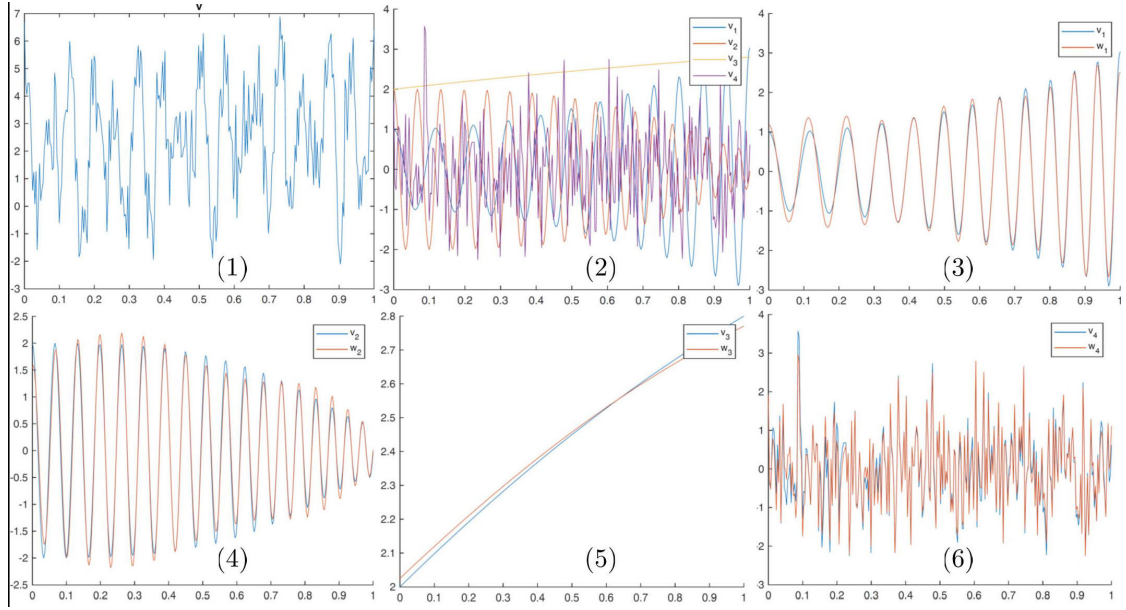
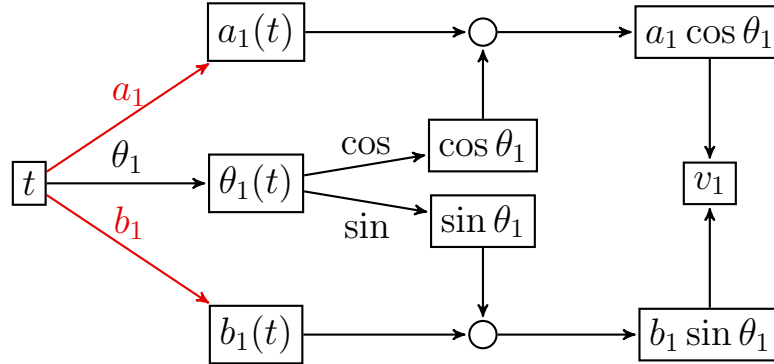


FIGURE 9. [28, Fig. 3.2]. (1) The signal $v = v_1 + v_2 + v_3 + v_4$ (2) The modes v_1, v_2, v_3, v_4 (3) v_1 and its approximation w_1 (4) v_2 and its approximation w_2 (5) v_3 and its approximation w_3 (6) v_4 and its approximation w_4 .

unknown functions a_i, b_i and the known functions $\cos(\theta_i), \sin(\theta_i)$.



6.7. Dynamic Computational Graph Completion. The process, presented in Sec. 6.6, of programming kernels via a computational graph by decomposing and recomposing simpler kernels is generic [28] and can be employed to design the computation graph itself. As an example, using the notations of Sec. 6.6, consider the classical empirical mode decomposition problem [16] of recovering (v_1, \dots, v_m) (Fig. 11.5-7) from the data $(\mathbf{t}, v(\mathbf{t}))$ (Fig. 11.1) where $v = v_\sigma + \sum_{i=1}^m v_i$. In that problem, m is unknown, v_σ is white noise and the v_i are of the form $v(t) = a_i(t) \cos(\theta_i(t))$ where the a_i are piecewise smooth unknown functions and the instantaneous frequencies $\dot{\theta}_i$ are strictly positive, well separated and unknown smooth functions.

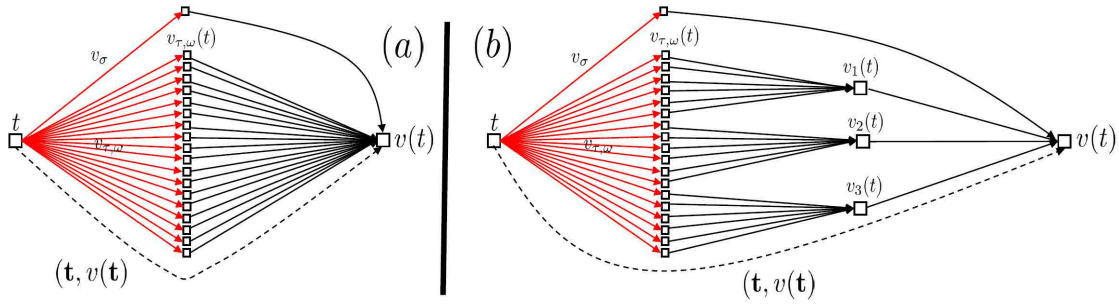


FIGURE 10. CGC diagrams for empirical mode decomposition. (a) Recovery of the fine modes $v_{\tau,\omega}$ (b) Recovery of the coarse modes v_i through aggregation of the fine modes $v_{\tau,\omega}$.

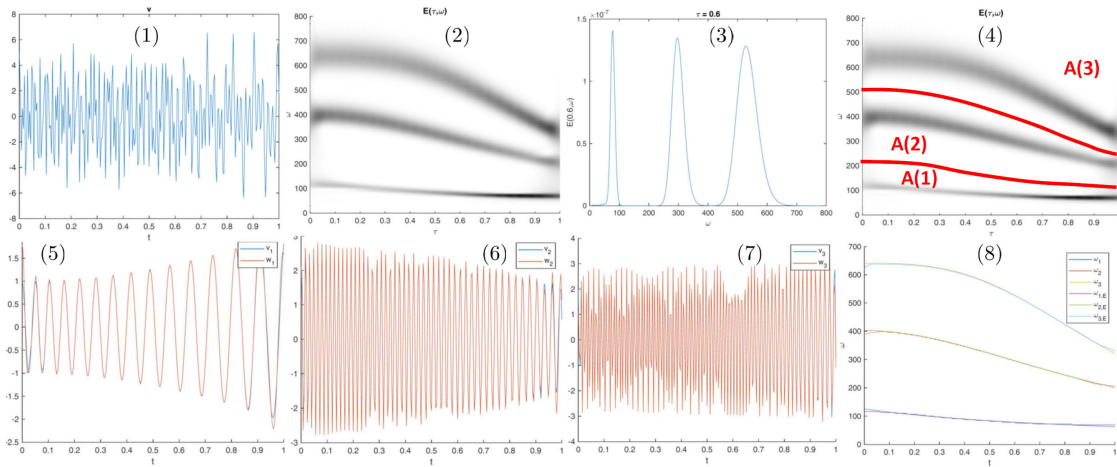


FIGURE 11. [28, Fig. 4.10]. (1) The signal $v = u + v_{\sigma}$ where $u = v_1 + v_2 + v_3$, $v_{\sigma} \sim \mathcal{N}(0, \sigma^2 \delta(t - s))$ and $\sigma = 0.01$ (2) $(\tau, \omega) \rightarrow E(\tau, \omega)$ defined by (6.32) (one can identify three stripes) (3) $\omega \rightarrow E(0.6, \omega)$ (4) Partitioning $[0, 1] \times [\omega_{\min}, \omega_{\max}] = \cup_{i=1}^3 A_i$ of the time frequency domain into three disjoint subsets identified from E (5) v_1 and its approximation w_1 (6) v_2 and its approximation w_2 (7) v_3 and its approximation w_3 (8) $\omega_{1,E}, \omega_{2,E}, \omega_{3,E}$.

Then, as shown in [28], the v_i can be recovered through a hierarchical and dynamic programming approach to the design of a computational graph (of the type presented in Sec. 6.6). In this approach the v_i are identified as aggregates (integrals/sums, see Fig. 10.(b)) of finer/simpler modes, i.e.

$$v_i(t) = \sum_{(\tau,\omega) \in A_i} v_{\tau,\omega}(t), \quad (6.26)$$

where the A_i are an unknown partition of the time-frequency domain spanned by (τ, ω) , and,

$$v_{\tau,\omega}(t) = a_{\tau,\omega} \chi_{\tau,\omega,c}(t) + b_{\tau,\omega} \chi_{\tau,\omega,s}(t) \quad (6.27)$$

where the a and b are unknown functions and the χ are Gabor wavelets defined by

$$\begin{aligned}\chi_{\tau,\omega,c}(t) &:= \left(\frac{2}{\pi}\right)^{\frac{1}{4}} \sqrt{\frac{\omega}{\alpha}} \cos(\omega(t-\tau)) e^{-\frac{\omega^2(t-\tau)^2}{\alpha^2}}, \quad t \in \mathbb{R}, \\ \chi_{\tau,\omega,s}(t) &:= \left(\frac{2}{\pi}\right)^{\frac{1}{4}} \sqrt{\frac{\omega}{\alpha}} \sin(\omega(t-\tau)) e^{-\frac{\omega^2(t-\tau)^2}{\alpha^2}}, \quad t \in \mathbb{R}.\end{aligned}\quad (6.28)$$

Observing that

$$\sum_{(\tau,\omega)} v_{\tau,\omega}(t) = v(t), \quad (6.29)$$

the recovery of the unknown functions a and b is a linear mode decomposition problem whose CGC diagram is illustrated in Fig. 10.(a). Replacing a and b by white noise leads to the approximation of $v_{\tau,\omega}$ with

$$w_{\tau,\omega}(t) = \sum_{\mathbf{t}} K_{\tau,\omega}(t, \mathbf{t}) K(\mathbf{t}, \mathbf{t})^{-1} v(\mathbf{t}), \quad (6.30)$$

where $K = \sum_{\tau,\omega} K_{\tau,\omega}$ and

$$K_{\tau,\omega}(t, t') = \chi_{\tau,\omega,c}(t) \chi_{\tau,\omega,c}(t') + \chi_{\tau,\omega,s}(t) \chi_{\tau,\omega,s}(t'). \quad (6.31)$$

To identify the unknown partition formed by the subsets A_i (i.e., the connectivity of the graph illustrated in Fig. 10.(b)), we compute the inner product

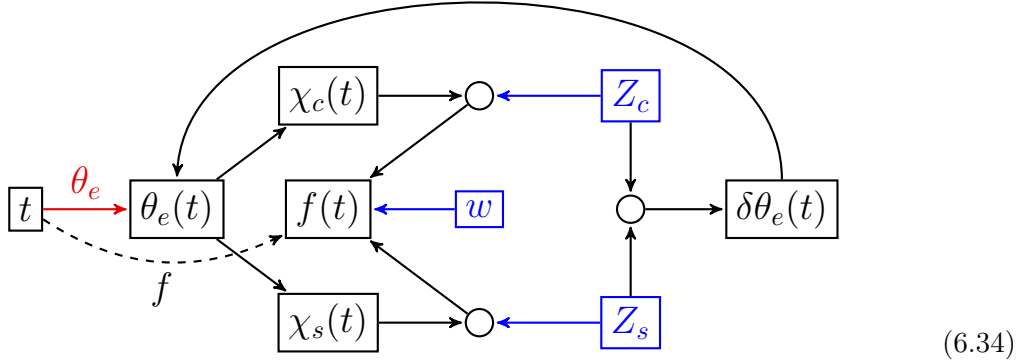
$$E(\tau, \omega) = (w_{\tau,\omega}(\mathbf{t}))^T K(\mathbf{t}, \mathbf{t})^{-1} v(\mathbf{t}). \quad (6.32)$$

This inner product is the variance of $(v_{\tau,\omega}(\mathbf{t}))^T K(\mathbf{t}, \mathbf{t})^{-1} v(\mathbf{t})$ when the coefficients $a_{\tau,\omega}$ and $b_{\tau,\omega}$ of $v_{\tau,\omega}$ are randomized as white noise and can be interpreted as the level of activation of the resulting GP $v_{\tau,\omega}$ after conditioning on the data.

Figure 11 ([28, Fig. 4.10]) illustrates the proposed approach for a noisy signal composed of three quasi-trigonometric modes (the fourth mode is white noise). Figure 11.1 displays the total observed signal v and the three quasi-trigonometric modes v_1, v_2, v_3 constituting v are displayed in Figures 11.5, 6 and 7, along with their recoveries w_1, w_2 and w_3 . Figure 11.8 also shows approximations of the instantaneous frequencies obtained as

$$\omega_{i,E}(t) := \operatorname{argmax}_{\omega:(t,\omega) \in A_i} E(t, \omega). \quad (6.33)$$

6.8. Cyclic Graph. In the following example, taken from [28], we illustrate a CGC problem involving a cyclic graph. The underlying algorithm is used in [28, Chap. 6] to solve empirical mode decomposition problems (as described in Sec. 6.7, with possibly unknown non-trigonometric waveforms) to near machine precision. The CGC diagram of this algorithm is illustrated by the following diagram.



To describe it, let τ a given time, θ_e be an estimated phase function (to be refined), and a signal f . Suppose that f contains a mode of the form $a(t) \cos(\theta(t))$ near the time τ . The problem is to estimate a and θ near τ . The cycle in the graph allows us to do so by successively correcting/refining an initial estimate θ_e of θ . This is done by identifying an updated estimate $\theta_e(\tau) + \delta\theta(\tau)$ of θ by solving the following GP regression problem

$$(f(t) - X_c \cos(\theta_e(t)) - X_s \sin(\theta_e(t)) - w(t)) e^{-\left(\frac{\theta_e(\tau)(t-\tau)}{\alpha}\right)^2} = 0, \quad (6.35)$$

where w is white noise and X_c and X_s are independent $\mathcal{N}(0, 1)$ random variables. a and the correction $\delta\theta$ are then identified as

$$\begin{aligned} a(\tau) &:= \sqrt{X_c^2 + X_s^2} \\ \delta\theta(\tau) &:= \text{atan2}(-X_s, X_c). \end{aligned} \quad (6.36)$$

6.9. Incorporating symmetries. Unknown functions can be informed about underlying symmetries by employing equivariant kernels [32] and their generalization [25, Sec. 9.2]. Such kernels can be obtained by averaging a given kernel with respect to the action of a unitary group of transformations. From the perspective of CGC, convolutional neural networks can be recovered (see [25, Sec. 9.2]) by replacing unknown functions with GPs of the form

$$\xi = \frac{1}{|\mathcal{G}|} \sum_{g \in \mathcal{G}} g^T R^T \xi_g(Pgx) \quad (6.37)$$

where the ξ_g are independent GPs, \mathcal{G} is a finite group of unitary transformations, $|\mathcal{G}|$ is its volume with respect to the Haar measure, P and R are linear projection operators.

Acknowledgments. The author gratefully acknowledges partial support by the Air Force Office of Scientific Research under MURI award number FA9550-20-1-0358 (Machine Learning and Physics-Based Modeling and Simulation). Thanks to Amy Braverman, Jouni Susiluoto, and Otto Lamminpää for stimulating discussions.

References

- [1] Pierre Baldi. Autoencoders, unsupervised learning, and deep architectures. In *Proceedings of ICML workshop on unsupervised and transfer learning*, pages 37–49. JMLR Workshop and Conference Proceedings, 2012.
- [2] Mikhail Belkin. Fit without fear: remarkable mathematical phenomena of deep learning through the prism of interpolation. *arXiv preprint arXiv:2105.14368*, 2021.
- [3] Lisa Gottesfeld Brown. A survey of image registration techniques. *ACM computing surveys (CSUR)*, 24(4):325–376, 1992.
- [4] Yifan Chen, Bamdad Hosseini, Houman Owhadi, and Andrew M Stuart. Solving and learning nonlinear pdes with gaussian processes. *Journal of Computational Physics*, 2021. arXiv preprint arXiv:2103.12959.
- [5] Yifan Chen, Houman Owhadi, and Andrew Stuart. Consistency of empirical bayes and kernel flow for hierarchical parameter estimation. *Mathematics of Computation*, 2021.
- [6] Jon Cockayne, Chris J Oates, Timothy John Sullivan, and Mark Girolami. Bayesian probabilistic numerical methods. *SIAM Review*, 61(4):756–789, 2019.
- [7] P. G. Constantine, E. Dow, and Q. Wang. Active subspace methods in theory and practice: applications to kriging surfaces. *SIAM Journal on Scientific Computing*, 36(4):A1500–A1524, 2014.
- [8] Noel Cressie. Spatial prediction and ordinary kriging. *Mathematical geology*, 20(4):405–421, 1988.
- [9] Dieter Fensel, U Simsek, Kevin Angele, Elwin Huaman, Elias Kärle, Oleksandra Panasiuk, Ioan Toma, Jürgen Umbrich, and Alexander Wahler. *Knowledge graphs*. Springer, 2020.
- [10] Gene H Golub and Christian Reinsch. Singular value decomposition and least squares solutions. In *Linear algebra*, pages 134–151. Springer, 1971.
- [11] Ulf Grenander and Michael I Miller. Computational anatomy: An emerging discipline. *Quarterly of applied mathematics*, 56(4):617–694, 1998.
- [12] B Hamzi, R Maulik, and H Owhadi. Simple, low-cost and accurate data-driven geophysical forecasting with learned kernels. *Proceedings of the Royal Society A*, 477(2252):20210326, 2021.
- [13] Boumediene Hamzi and Houman Owhadi. Learning dynamical systems from data: A simple cross-validation perspective, part i: Parametric kernel flows. *Physica D: Nonlinear Phenomena*, 421:132817, 2021.
- [14] Kaiming He, Xiangyu Zhang, Shaoqing Ren, and Jian Sun. Deep residual learning for image recognition. In *Proceedings of the IEEE conference on computer vision and pattern recognition*, pages 770–778, 2016.
- [15] P. Hennig, M. A. Osborne, and M. Girolami. Probabilistic numerics and uncertainty in computations. *Proc. R. Soc. A.*, 471(2179):20150142, 2015.
- [16] N. E. Huang, Z. Shen, S. R. Long, M. C. Wu, H. H. Shih, Q. Zheng, N.-C. Yen, C. C. Tung, and H. H. Liu. The empirical mode decomposition and the Hilbert spectrum for nonlinear and non-stationary time series analysis. *Proceedings of the Royal Society of London. Series A: Mathematical, Physical and Engineering Sciences*, 454(1971):903–995, 1998.
- [17] Michael Irwin Jordan. *Learning in graphical models*, volume 89. Springer Science & Business Media, 1998.
- [18] Yankai Lin, Zhiyuan Liu, Maosong Sun, Yang Liu, and Xuan Zhu. Learning entity and relation embeddings for knowledge graph completion. In *Twenty-ninth AAAI conference on artificial intelligence*, 2015.
- [19] C. A. Micchelli and T. J. Rivlin. A survey of optimal recovery. In *Optimal Estimation in Approximation Theory*, pages 1–54. Springer, 1977.
- [20] Sebastian Mika, Bernhard Schölkopf, Alexander J Smola, Klaus-Robert Müller, Matthias Scholz, and Gunnar Rätsch. Kernel pca and de-noising in feature spaces. In *NIPS*, volume 11, pages 536–542, 1998.
- [21] Natasha Noy, Yuqing Gao, Anshu Jain, Anant Narayanan, Alan Patterson, and Jamie Taylor. Industry-scale knowledge graphs: lessons and challenges. *Communications of the ACM*, 62(8):36–43, 2019.
- [22] H. Owhadi, C. Scovel, and F. Schäfer. Statistical Numerical Approximation. 66(10), 2019.

- [23] Houman Owhadi. Bayesian numerical homogenization. *Multiscale Modeling & Simulation*, 13(3):812–828, 2015.
- [24] Houman Owhadi. Multigrid with rough coefficients and multiresolution operator decomposition from hierarchical information games. *SIAM Review*, 59(1):99–149, 2017.
- [25] Houman Owhadi. Do ideas have shape? plato’s theory of forms as the continuous limit of artificial neural networks. *arXiv preprint arXiv:2008.03920*, 2020.
- [26] Houman Owhadi. Notes on operator valued kernels, feature maps and gaussian processes. 2021. http://users.cms.caltech.edu/~owhadi/index_htm_files/OperatorValuedGPs.pdf.
- [27] Houman Owhadi and Clint Scovel. *Operator-Adapted Wavelets, Fast Solvers, and Numerical Homogenization: From a Game Theoretic Approach to Numerical Approximation and Algorithm Design*, volume 35. Cambridge University Press, 2019.
- [28] Houman Owhadi, Clint Scovel, and Gene Ryan Yoo. *Kernel Mode Decomposition and the programming of kernels*. Springer, 2021. arXiv preprint arXiv:1907.08592 for early version.
- [29] Houman Owhadi and Gene Ryan Yoo. Kernel flows: From learning kernels from data into the abyss. *Journal of Computational Physics*, 389:22–47, 2019.
- [30] M. Raissi, P. Perdikaris, and G. E. Karniadakis. Inferring solutions of differential equations using noisy multi-fidelity data. *Journal of Computational Physics*, 335:736–746, 2017.
- [31] Maziar Raissi, Paris Perdikaris, and George E Karniadakis. Physics-informed neural networks: A deep learning framework for solving forward and inverse problems involving nonlinear partial differential equations. *Journal of Computational Physics*, 378:686–707, 2019.
- [32] Marco Reiser and Hans Burkhardt. Learning equivariant functions with matrix valued kernels. *Journal of Machine Learning Research*, 8(Mar):385–408, 2007.
- [33] Florian Schäfer, Matthias Katzfuss, and Houman Owhadi. Sparse cholesky factorization by kullback–leibler minimization. *SIAM Journal on Scientific Computing*, 43(3):A2019–A2046, 2021.
- [34] Bernhard Scholkopf and Alexander J Smola. *Learning with kernels: support vector machines, regularization, optimization, and beyond*. MIT Press, 2018.
- [35] Nitish Srivastava, Geoffrey Hinton, Alex Krizhevsky, Ilya Sutskever, and Ruslan Salakhutdinov. Dropout: a simple way to prevent neural networks from overfitting. *The journal of machine learning research*, 15(1):1929–1958, 2014.
- [36] Gottfried Tinhofer, Rudolf Albrecht, Ernst Mayr, Hartmut Noltemeier, and Maciej M Syslo. *Computational graph theory*, volume 7. Springer Science & Business Media, 2012.
- [37] Christopher K. I. Williams and Carl Edward Rasmussen. *Gaussian Processes for Machine Learning*. The MIT Press, 2006.
- [38] Gene Ryan Yoo and Houman Owhadi. Deep regularization and direct training of the inner layers of neural networks with kernel flows. *arXiv preprint arXiv:2002.08335*, 2020.
- [39] Laurent Younes. *Shapes and diffeomorphisms*, volume 171. Springer, 2010.